

# JGR Atmospheres

## RESEARCH ARTICLE

10.1029/2020JD033942

### Key Points:

- Inclusion of brown carbon (BrC) in a modified bulk aerosol optical scheme enhances the simulated surface absorption of aerosol
- BrC inclusion improves the agreement between simulated aerosol optical properties and observations in biomass burning site
- Refractive index of BrC, size and mixing state of aerosol are major contributors to uncertainties in optical simulation in two Asian sites

### Supporting Information:

Supporting Information may be found in the online version of this article.

### Correspondence to:

Y. Peng,  
pyiran@mail.tsinghua.edu.cn

### Citation:

Xu, L., Peng, Y., Ram, K., Zhang, Y., Bao, M., & Wei, J. (2021). Investigation of the uncertainties of simulated optical properties of brown carbon at two Asian sites using a modified bulk aerosol optical scheme of the Community Atmospheric Model version 5.3. *Journal of Geophysical Research: Atmospheres*, 126, e2020JD033942. <https://doi.org/10.1029/2020JD033942>

Received 22 SEP 2020  
Accepted 22 JUN 2021

### Author Contributions:

**Conceptualization:** Lulu Xu, Yiran Peng  
**Data curation:** Lulu Xu, Kirpa Ram, Mengying Bao  
**Formal analysis:** Lulu Xu  
**Funding acquisition:** Yiran Peng, Kirpa Ram, Yanlin Zhang  
**Investigation:** Lulu Xu, Jing Wei  
**Methodology:** Lulu Xu, Yiran Peng, Jing Wei  
**Resources:** Yiran Peng, Kirpa Ram, Yanlin Zhang  
**Writing – original draft:** Lulu Xu, Yiran Peng, Kirpa Ram, Mengying Bao, Jing Wei  
**Writing – review & editing:** Lulu Xu, Yiran Peng, Kirpa Ram

© 2021. American Geophysical Union.  
All Rights Reserved.

## Investigation of the Uncertainties of Simulated Optical Properties of Brown Carbon at Two Asian Sites Using a Modified Bulk Aerosol Optical Scheme of the Community Atmospheric Model Version 5.3

Lulu Xu<sup>1</sup> , Yiran Peng<sup>1</sup> , Kirpa Ram<sup>2</sup> , Yanlin Zhang<sup>3</sup> , Mengying Bao<sup>3</sup>, and Jing Wei<sup>4</sup> 

<sup>1</sup>Ministry of Education Key Laboratory for Earth System Modeling, Department of Earth System Science, Tsinghua University, Beijing, China, <sup>2</sup>Institute of Environment and Sustainable Development, Banaras Hindu University, Varanasi, India, <sup>3</sup>Yale-NUIST Center on Atmospheric Environment, Nanjing University of Information Science and Technology, Nanjing, China, <sup>4</sup>Department of Chemical and Biochemical Engineering, Iowa Technology Institute, Center for Global and Regional Environmental Research, University of Iowa, Iowa City, IA, USA

**Abstract** Recent studies have suggested that brown carbon (BrC), an absorbing component in organic aerosol, has strong absorption in the near-ultraviolet wavelengths, and contributes to regional and global radiative forcing (RF). However, the inclusion of BrC in global climate models leads to significant uncertainties in estimated RF, mainly attributed to uncertain BrC properties and relevant BrC parameters assigned in the model. In this study, we modified the bulk aerosol optical scheme (BAOS) in Community Atmospheric Model version 5.3 by including BrC absorption and evaluated the performance of the modified BAOS by comparing the simulated aerosol absorption with 2-year surface observational data in two Asian cities, Kanpur, India and Nanjing, China. The mean relative errors in the simulated total aerosol absorption ( $B_{abs}$ ) and absorption Angstrom exponent in modified BAOS are around 35% in Kanpur and even below 20% in Nanjing. Our results show that the inclusion of BrC remedies the underestimated total aerosol absorption by 20% and 14% on average at Kanpur and Nanjing, respectively, exhibiting a better agreement with ground-based observations of aerosol absorption at both sites. We also conducted a series of sensitivity experiments to quantify the uncertainties caused by varying parameters related to BrC. The model simulations suggest that the imaginary refractive index of BrC is the most significant factor contributing to the uncertainties in aerosol optical properties calculated in BAOS at the Kanpur site. While in the Nanjing site, both particle size distribution and mixing state have dominant impacts on the calculated aerosol optical properties.

**Plain Language Summary** Observed existence of absorbing part in organic carbon, referred to as “brown carbon (BrC),” inspired scientists to rethink the climate effect of organic aerosols. Current climate models included BrC in aerosol calculation in an oversimplified way. We use aerosol data from field measurements in two Asian sites to evaluate some parameters of BrC properties in the aerosol calculation. Our results show that absorptivity of BrC is most important for biomass burning region where wild fires prevail, and aerosol particle size and mixing features are most important for urban region where pollutions from human activities are dominant. We claim that seasonally varying and location dependent parameters for representing BrC properties will benefit to more accurate calculations of organic aerosol and its climate effect in model.

## 1. Introduction

Many studies in recent decades have shown that an absorbing component exists in organic carbon (OC) (Alexander et al., 2008; Bond, 2001; Kirchstetter & Thatcher, 2012; Satish et al., 2017), which is known as brown carbon (BrC). BrC absorbs strongly in near-ultraviolet wavelengths lower than 400 nm (Hoffer et al., 2006; Kirchstetter et al., 2004; Roden et al., 2006). BrC has diverse sources. One is “primary BrC” from biomass burning (Chakrabarty et al., 2010; Lack et al., 2012), smoldering fires, and biogenic release of humic matter (Andreae & Gelencsér, 2006; Rizzo et al., 2013). The other is “secondary BrC” from photochemical oxidation and multi-phase reactions (A. K. Y. Lee et al., 2013; Powelson et al., 2013; Updyke et al., 2012).

Diverse sources and uncertain chemical components cause a wide range of BrC optical properties (e.g., imaginary refractive index [RI],  $K_{\text{BrC}}$  and mass absorption efficiency, MAE,  $\text{m}^2 \text{ g}^{-1}$ ). Previous studies have tried to measure the optical parameters of BrC by directly using in situ observations and indirectly utilizing Mie calculation model. However, the current values of  $K_{\text{BrC}}$  still range in two orders of magnitude in the near-ultraviolet wavelengths (Chakrabarty et al., 2010; Hoffer et al., 2006; Lack et al., 2012; J. M. Liu et al., 2013; Saleh et al., 2013; Shamjad et al., 2016). On the other hand, BrC concentrations in the atmosphere cannot be directly measured and are commonly retrieved from optical measurements (Arola et al., 2011; Chen & Bond, 2010; Feng et al., 2013; Park et al., 2010). Thus the mass fraction of BrC in OC is highly uncertain. In addition, BrC could exist in soluble or insoluble OC, or both (Chen & Bond, 2010; Cheng et al., 2011; Hoffer et al., 2006; Laskin et al., 2015; J. M. Liu et al., 2013; Satish et al., 2017; Yan et al., 2017; Zeng et al., 2020). Mixing state of BrC with other aerosol species also adds complexity in the calculation of BrC optical properties. Some studies indicate that black carbon (BC) core coated by scattering aerosols (e.g., sulfate and OC) might lead to an enhancement of absorption by a factor of two, which is called the lensing effect (Bond & Bergstrom, 2006; Haywood & Shine, 1995; Jacobson, 2000, 2001). If absorbing components such as BrC are included in the coating shell, the lensing effect will be reduced by 25%–50% (Lack & Cappa, 2010; Saleh et al., 2015).

All the above-mentioned uncertainties bring difficulties in understanding BrC impacts on climate. Both regional and global radiative effects of BrC have been estimated by a number of studies using chemical transport models (CTMs) coupled with radiative transfer models or global climate models (Brown et al., 2018; Feng et al., 2013; Lin et al., 2014; Park et al., 2010; X. Wang et al., 2018; A. Zhang et al., 2020). There are usually two methods to calculate the absorption of BrC in model. First, some studies separated BrC from OC and used the assumed values of  $K_{\text{BrC}}$  or MAE, mass concentration fraction, and/or mixing strategy for BrC. For example, Park et al. (2010) considered the absorption of BrC in a CTM by using a BrC/BC ratio of unity and MAE value of  $3.8 \text{ m}^2 \text{ g}^{-1}$  from Alexander et al. (2008). Feng et al. (2013) assumed 66% of biomass and biofuel OC as BrC and used two sets of  $K_{\text{BrC}}$  values (0.003 and 0.03 at 550 nm as moderate and strong  $K_{\text{BrC}}$ , respectively) for including BrC in a CTM. Lin et al. (2014) also assumed the same moderate and strong  $K_{\text{BrC}}$  values in a CTM as Feng et al. (2013), but BrC mass was proportional to all primary and secondary OC. X. Wang et al. (2014) assumed 25% of biomass burning and 50% of biofuel POA (primary OA) as well as aromatic SOA (secondary OA) were brown, MAE at 440 nm was  $1.0 \text{ m}^2 \text{ g}^{-1}$  for POA and  $0.3 \text{ m}^2 \text{ g}^{-1}$  for SOA. A. Zhang et al. (2020) used constant MAE values for brown POA ( $1.0 \text{ m}^2 \text{ g}^{-1}$  at 550 nm) and SOA ( $0.19 \text{ m}^2 \text{ g}^{-1}$  at 550 nm) and a derived BrC global biomass burning emission inventory. The various assumptions in BrC properties lead to high uncertainties in the BrC radiative forcing (RF). The estimated global direct radiative effects (DRE) of BrC in top of atmosphere range from  $0.04 \text{ W m}^{-2}$  to  $0.57 \text{ W m}^{-2}$  (Feng et al., 2013; Lin et al., 2014; Park et al., 2010). However, these studies hardly discriminate which BrC parameter is most responsible for the uncertainties in aerosol optical calculations and DRE estimation in climate models.

Second, other modeling studies did not separate BrC from OC but connected BrC absorption to a BC-to-OA ratio (Brown et al., 2018; Saleh et al., 2015; X. Wang et al., 2018) since BrC absorption from biofuel or biomass sources is likely affected by combustion conditions (Lu et al., 2015; Saleh et al., 2014). Saleh et al. (2015) applied this method, which did not explicitly give the optical parameters of BrC in the model, but parameterized imaginary RI of OA ( $K_{\text{OA}}$ ) as a function of the columnar mass burden of BC-to-OA (here OA = POA + SOA) ratio in a CTM and ran a radiative transfer model to estimate the global RF of carbonaceous aerosol. Saleh et al. (2015) showed that the global mean DRE due to OA absorption (equivalent to BrC absorption) is  $+0.22 \text{ W m}^{-2}$  and  $+0.12 \text{ W m}^{-2}$  for external and internal mixing cases, respectively. Brown et al. (2018) utilized a similar method as Saleh et al. (2015) but parameterizing  $K_{\text{OA}}$  as a function of the columnar mass burden of BC to POA. They obtained a global BrC DRE of  $0.13 \pm 0.01 \text{ W m}^{-2}$ . However, this method has limitations given the lack of information regarding burn conditions in emission inventories. The parameterization of  $K_{\text{OA}}$  as a function of BC-to-OA ratio implied that BrC experienced the same physical processes of transport, deposition, and mixing as OA in model. However, aircraft measurements in Y. Zhang et al. (2017) indicated that BrC and nonabsorbing OA behaved very differently in wet deposition and vertical distribution. Therefore, we believe that the explicit presentations of BrC properties are still necessary for the climate model because BrC and nonabsorbing OA should be separately simulated in terms of aerosol physical and optical processes.

A major role of model studies mentioned above is to assess the RF of BrC with verifications on the total aerosol optics (e.g.,  $B_{\text{abs}}$ , absorption Angstrom exponent [AAE], absorbing aerosol optical depth) using measurements from field campaigns (Park et al., 2010) or Aerosol Robotic Network (AERONET) (Brown et al., 2018; Feng et al., 2013; Lin et al., 2014). However, noticeable discrepancies in aerosol optics between model outputs and observations still exist, yet few studies have tried to identify the sources of uncertainties in BrC simulation. Because current models have limited abilities in simulating the physical life cycle and reproducing the temporal-spatial distribution of BrC aerosol (mostly due to the limited observational information about the chemical, physical and optical properties of BrC aerosol, thus the oversimplified BrC parameters applied in model). In most model studies, the globally uniform and time-invariant values are prescribed for BrC parameters such as the mass ratio of BrC to OC, the imaginary RI of BrC, or mixing state of BrC with other aerosol species based on field measurements or lab experiments (e.g., Feng et al., 2013; Lin et al., 2014; X. Wang et al., 2014; A. Zhang et al., 2020). Therefore, we isolate the aerosol optical calculation in a GCM and try to rule out the possible uncertainty sources from emissions and physical calculation of aerosol species other than BrC, focusing on the BrC related parameters and evaluating their respective contributions to uncertainties in the simulated aerosol optical properties.

In this study, we modify the bulk aerosol optical scheme (BAOS) of the Community Atmosphere Model version 5.3 (CAM5.3) by including BrC in the aerosol optical calculation. Aerosol chemical components, mass concentrations, and aerosol absorptive properties from measurements were collected in two surface sites in India and China respectively. We use the observed aerosol mass concentrations as inputs for the modified BAOS, in order to rule out the possible uncertainties introduced from the model emission or physical calculations of aerosol. The observed aerosol absorptive properties are used to evaluate the performance of the modified BAOS. We also conduct a series of sensitivity experiments to quantify the potential contributions of BrC parameters to the uncertainties of total aerosol absorption in the modified BAOS. Sensitivity experiments will help to identify which BrC parameter causes the largest uncertainties in the optical scheme. Combining modeling work with measurement data, we expect the current study will shed a light on the sources of uncertainties in the simulated BrC absorption in the climate model. Future observational studies could refer to this work and aim to provide more accurate measurements of the most influencing BrC parameter to model. From the modeling perspective, the modified BAOS with the inclusion of BrC can be utilized in current GCM to enhance the accuracy of the aerosol optical calculation. It will also help to reduce the uncertainties in the estimated BrC effect on climate.

Materials of this study are organized as below: the measurement data of aerosol chemical compositions and aerosol absorption in Kanpur and Nanjing sites are presented in Section 2. BAOS, as well as modifications on the scheme, are introduced in Section 3. Methodology of the closure check and setup of sensitivity experiments are described in Section 4. Analyses of simulated results are exhibited in Section 5. Lastly, Section 6 gives conclusions and discussions.

## 2. Measurement Data

### 2.1. Site Description

Surface aerosol and relative humidity (RH) data were collected at two sites, in Kanpur, India ( $26.5^{\circ}\text{N}$ ,  $80.3^{\circ}\text{E}$ , 142 m above mean sea level) from January 2007 to February 2008 and in Nanjing, China ( $32.2^{\circ}\text{N}$ ,  $118.7^{\circ}\text{E}$ , 22 m above mean sea level) from October 2015 to April 2017. The sampling site in Kanpur was set up inside the campus of Indian Institute of Technology, located in the center of the Indo-Gangetic plain. Although fossil-fuel (vehicles and industries) and biofuel (wood fuel, leaves, and agricultural waste, etc.) emissions are the main sources of carbonaceous aerosols, the emission strength, as well as composition, exhibits a strong seasonal variability (Bikkina et al., 2017; Ram et al., 2010a). Based on  $\text{K}^{+}$  concentrations and selected tracers/ratios (e.g., OC/EC,  $\text{K}^{+}/\text{OC}$  ratios), biomass burning emission (wood-fuels and agricultural waste) has been identified as a major source of carbonaceous aerosols during wintertime over northern India (Ram & Sarin, 2015). Based on robust measurements of  $^{14}\text{C}$  in aerosol samples from Kanpur, Bikkina et al. (2017) reported seasonal variability in biomass burning emissions with a higher contribution in fall and winter and a reduced contribution in spring and summer. The sampling site at Nanjing was set up in Nanjing University of Information Science and Technology (NUIST), located in the central part of the Yangtze River Delta region of China. Surrounding the campus are highway and heavy polluting enterprises, thus traffic and

industrial air pollution are severe. The duration of sampling was 11 and 10 months in Kanpur and Nanjing, respectively. Data were often missing in June, July, August, and September due to heavy precipitation in the summer monsoon season.

## 2.2. Particulate Matters

Table S1 gives a summary of instruments and data information for this study. Analytical measurements of ambient aerosols ( $\text{PM}_{10}$ , particulate matter with aerodynamic diameter  $< 10 \mu\text{m}$ ) in Kanpur have been described in Ram et al. (2010a). All samples were collected during the daytime and integrated for every 8–10 h. In Nanjing, the  $\text{PM}_{10}$  concentrations were measured using the Tapered Element Oscillating Microbalance (TEOM1405-DF, ThermoFisher Scientific, America). The interval of measured data was 6 min. The instrumental operational maintenance, data assurance, and quality control were performed according to the Chinese Ministry of Environmental Protection Standards for  $\text{PM}_{10}$  and PM2.5 which was named “HJ 655-2013” (Y. L. Zhang & Cao, 2015). We averaged the  $\text{PM}_{10}$  data in both sites to monthly means. In this study, we use the measurement data for evaluating a scheme of aerosol optical calculation for applying in a climate model thus only investigate monthly mean data.

## 2.3. Measured Chemical Compositions

The mass concentrations of OC and elemental carbon (EC) in ambient aerosols at both sites were assessed by a semi-continuous carbon analyzer (OC/EC analyzer) (Model-4, Sunset Laboratory, America) using NI-OSH-5040 (National Institute of Occupational Safety and Health) protocol based on the thermal-optical transmittance method. The analytical details of the OC/EC analyzer were described in an earlier publication (Ram et al., 2008). In the Kanpur site, the analyzer was operated offline with a sampling period of 8–10 h and one laser (678 nm). In the Nanjing site, the OC/EC analyzer was utilized online with two lasers (405 and 658 nm) and the sampling period is 1 h. The mass concentrations of water-soluble OC (WSOC) in both sites were analyzed through a total OC (TOC) analyzer (Shimadzu-TOC-V<sub>CPH</sub>, Shimadzu, Japan) (Kirillova et al., 2010).

Water-soluble cations ( $\text{Na}^+$ ,  $\text{K}^+$ ,  $\text{NH}_4^+$ ,  $\text{Ca}^{2+}$ , and  $\text{Mg}^{2+}$ ) and anions ( $\text{Cl}^-$ ,  $\text{SO}_4^{2-}$ , and  $\text{NO}_3^-$ ) in aerosol were analyzed by ion chromatography (ThermoFisher Scientific, America) at both sampling sites (X. Liu et al., 2019; Ram et al., 2010a). Aerosol samples were collected from January 2007 to February 2008 at Kanpur (every 5th day), and from October to November in 2015 (every 12 h) at Nanjing. In addition, ionic species were measured by an online Monitor for AeRosols & Gases in Ambient Air (MARGA, Metrohm, Switzerland) with the time interval of 1 h from March to May, July 2016 and from January to April 2017 at Nanjing. A detailed description of the MARGA instrument is given in previous publications (Nie et al., 2015; Schaap et al., 2011). Meteorological parameters, including RH, were recorded with automatic weather stations near the two measuring sites.

## 2.4. Measurements of Aerosol Absorption Coefficient

Two analytical instruments, a 7- $\lambda$  Aethalometer (370, 470, 520, 590, 660, 880, and 950 nm, Magee Scientific, America) and OC/EC analyzer (405 and 658 nm) were used in Kanpur and Nanjing respectively for measurement of total aerosol absorption coefficient ( $B_{\text{abs}}$ , in  $\text{Mm}^{-1}$ ). In Kanpur, the Aethalometer functioned optically and the measured  $B_{\text{abs}}$  were highly sensitive to the absorption of carbon aerosol and dust aerosol. Although mineral dust could have significant absorption at 440 nm (Mishra & Tripathi, 2008), there were no experimental data of dust absorption measurement in India during the period of this study. Nonetheless, it is pertinent to mention that the absorption from mineral aerosols (or dust) is very low at 670 nm (i.e., close to BC measurement wavelength) even when the hematite ( $\text{Fe}_2\text{O}_3$ ) fraction is as high as 6% (Mishra & Tripathi, 2008). Therefore,  $B_{\text{abs}}$  from Aethalometer is based on the assumption that absorption is solely due to light-absorbing carbon (Weingartner et al., 2003). OC/EC analyzer applied a thermal-optical method for measurements in Nanjing. It relies on the thermal evaluation of OC and EC at different temperatures and inter/oxidizing atmosphere wherein the initial absorbance/transmittance measured using an inbuilt laser source is used to define the split point between OC and EC (Ram et al., 2008). Furthermore, the difference

**Table 1**  
*Physical and Optical Parameters Prescribed in the Modified BAOS of CAM5.3*

	$r_{\text{mod}}$ ( $\mu\text{m}$ )	$\sigma$	$\rho$ ( $\text{g}/\text{cm}^3$ )	Hygroscopicity	RI (442–625 nm)
Sulfate	0.069	2.03	1.77	Hydrophilic	1.43–0.0i
BC	0.012	2.0	2.0	Hydrophobic	1.75–0.44i
Scattering OC	0.0212	2.24	1.8	Hydrophilic/phobic	1.53–0.0i
Dust	1.51	1.9	2.6	Hydrophobic	1.53–0.01i
Sea salt	1.75	2.03	2.2	Hydrophilic	1.49–0.0i
BrC	0.0212	2.24	1.569	Hydrophilic/phobic	1.55–0.016i

Note.  $\rho$  is the density of each aerosol species. Hygroscopicity has three options, hydrophilic, hydrophobic, and hydrophilic/phobic mixed. Total mass of scattering OC (BrC) is the sum of hydrophilic (soluble) and hydrophobic (insoluble) scattering OC (BrC). RI of sulfate, BC, and sea salt are referred to Hess et al. (1998), RI of dust referred to Zender et al. (2003) and RI of BrC referred to Shamjad et al. (2016).

Abbreviations: BAOS, bulk aerosol optical scheme; BC, black carbon; BrC, brown carbon; CAM5.3, Community Atmosphere Model version 5.3; OC, organic carbon; RI, refractive index.

between the measured absorption coefficient in the two instruments and the methods has been discussed by Ram et al. (2010b).

### 3. Bulk Aerosol Optical Scheme

#### 3.1. BAOS Description

This study utilizes the BAOS in Rapid Radiative Transfer Method for GCMs of the CAM5.3. In original BAOS, five chemical species of aerosol (sulfate, BC, OC, dust, and sea salt) are assumed externally mixed and lognormal size distribution is prescribed for each aerosol species with given parameters (number mode radius [ $r_{\text{mod}}$ ]; geometric standard deviation [ $\sigma$ ]) as shown in Table S2 (Hess et al., 1998; Neale et al., 2010; Zender et al., 2003), in accordance with the framework of CAM5.3. The method of BAOS was described in detail by Neale et al. (2010). A look-up table (LUT) embedded in BAOS includes aerosol optics (mass extinction efficiency  $Q_{\text{ext}}$  [ $\text{m}^2 \text{ g}^{-1}$ ], mass scattering efficiency  $Q_{\text{sca}}$  [ $\text{m}^2 \text{ g}^{-1}$ ], and MAE  $Q_{\text{abs}}$  [ $\text{m}^2 \text{ g}^{-1}$ ]) of each aerosol species in 14 shortwave bands over the solar spectrum and in 10 RH bins. Inputs to BAOS are simulated RH and mass concentrations of the five aerosols species (and the partition between hydrophilic and hydrophobic OC) in the aerosol physical part of CAM5.3. Aerosol optical properties are obtained by integrating the optics with the simulated aerosol mass concentration, and then BAOS outputting extinction coefficients ( $B_{\text{ext}}$ , in  $\text{Mm}^{-1}$ ), scattering coefficients ( $B_{\text{sca}}$ , in  $\text{Mm}^{-1}$ ), absorption coefficients ( $B_{\text{abs}}$ , in  $\text{Mm}^{-1}$ ), and single scattering albedo (SSA).

#### 3.2. Modifications on BAOS

In this study, BrC is included as the sixth aerosol species to modify the BAOS, thus we must provide prescribed physical and optical parameters to representing BrC in BAOS. In the modified BAOS, we assumed that BrC had the same size distribution parameters as that of OC and the density of BrC was taken as  $1.569 \text{ g}/\text{cm}^3$  (Feng et al., 2013) (see Table 1). The remaining OC apart from BrC was regarded as the scattering OC. Scattering OC still had the same size distribution parameters, real RI and density as that of OC, while the imaginary RI of scattering OC was set to be 0. The density of BC was  $1.0 \text{ g}/\text{cm}^3$  in the original BAOS. Bond and Bergstrom (2006) suggested a larger value should be used based on measurements. Thus, we took  $2.0 \text{ g}/\text{cm}^3$  for BC density in the modified BAOS. As mentioned in the Introduction, BrC optical properties, mass concentrations, and mixing state with other aerosol species were prescribed as globally uniform and time-invariant values in model, but these parameters were highly uncertain and varying with time and location. Therefore we not only assigned BrC parameters in the model but also provided the range of parameter values for sensitivity experiments afterward. Note that the modified BAOS will be running standalone for this study, thus RH and mass concentrations of each aerosol species are provided by measurement data instead of transferred from the aerosol physical part of CAM5.3.

**Table 2**

*BrC Parameters and Assumptions in the Modified BAOS for Control Run and Sensitivity Experiments*

Experiment	$K_{\text{BrC}}$ (imaginary RI)			BrC/ WSOC mass ratio	Mixing assumption
	Band 11 (345– 442 nm)	Band 10 (442– 625 nm)	Band 9 (625– 778 nm)		
Control	0.037	0.016	0.001	50%	Core-Shell
Shell-nonBrC	0.037	0.016	0.001	0	Core-Shell
Low-abs	0.009	0.0019	0.001	50%	Core-Shell
High-abs	0.112	0.06	0.001	50%	Core-Shell
Sol-BrC	0.037	0.016	0.001	100%	Core-Shell
Ext-mix	0.037	0.016	0.001	50%	External

Abbreviations: BAOS, bulk aerosol optical scheme; BrC, brown carbon; RI, refractive index; WSOC, water-soluble OC.

### 3.2.1. Imaginary RI of BrC

BrC absorption in visible and near-ultraviolet bands are distinct as BrC absorption varies approximately with  $\lambda^{-2}$  to  $\lambda^{-9}$  ( $\lambda$  is the wavelength, Hecobian et al., 2010; Kirchstetter et al., 2004; J. Liu et al., 2015). However, no wavelength dependence of  $K_{\text{BrC}}$  within the fixed shortwave band is allowed and we keep the configuration of shortwave bands with prescribed wavelength ranges in BAOS, as the goal of this study is to identify the major sources of uncertainties in aerosol optical calculation in current GCM. In the modified BAOS,  $K_{\text{BrC}}$  is prescribed in each of the three shortwave bands (see Table 2, wavelength ranges in 625–778 nm for band 9, 442–625 nm for band 10, and 345–442 nm for band 11 in BAOS). Real and imaginary RIs in other bands are the same as that of OC in original BAOS.  $K_{\text{BrC}}$  in band 10 and band 11 are taken from the estimations by Shamjad et al. (2016), and  $K_{\text{BrC}}$  in band 9 follows the value in Kirchstetter et al. (2004), which are used for the Control run of BAOS (Table 2). However,  $K_{\text{BrC}}$  values could have a wide range according to previous studies. The minimum and maximum of  $K_{\text{BrC}}$  from the literature search are applied for sensitivity experiments (Low-abs and High-abs run respectively). We will discuss more on  $K_{\text{BrC}}$  values in Section 4.2.  $K_{\text{BrC}}$  in other shortwave bands and the RI of scattering OC in modified BAOS are kept the same as those of OC in original BAOS.

### 3.2.2. Mass Assignment of BrC

In the modified BAOS, BrC mass concentrations are obtained by assigning a certain ratio of OC to BrC. This is a simplified assumption because most current GCMs cannot explicitly separate the emission and physical processes of OC and BrC. We prescribe 50% mass of WSOC as BrC (Control run in Table 2). The fraction of BrC/WSOC (fBrC) varies from 0% to 100% for sensitivity check. More discussions on BrC mass assumption are presented in Section 4.2. To obtain BrC mass concentrations, the observed WSOC mass onsite is read in to drive the standalone BAOS. The monthly mean WSOC/OC ratios measured in Kanpur and Nanjing are shown in Figure 1. The ratios range from 0.3 to 0.6 during the entire sampling period and are higher in spring and summer for both sites. It is likely due to the high photochemical activity and oxidizing radical concentration promoting secondary organic aerosol formation during warmer seasons (Ram & Sarin, 2015).

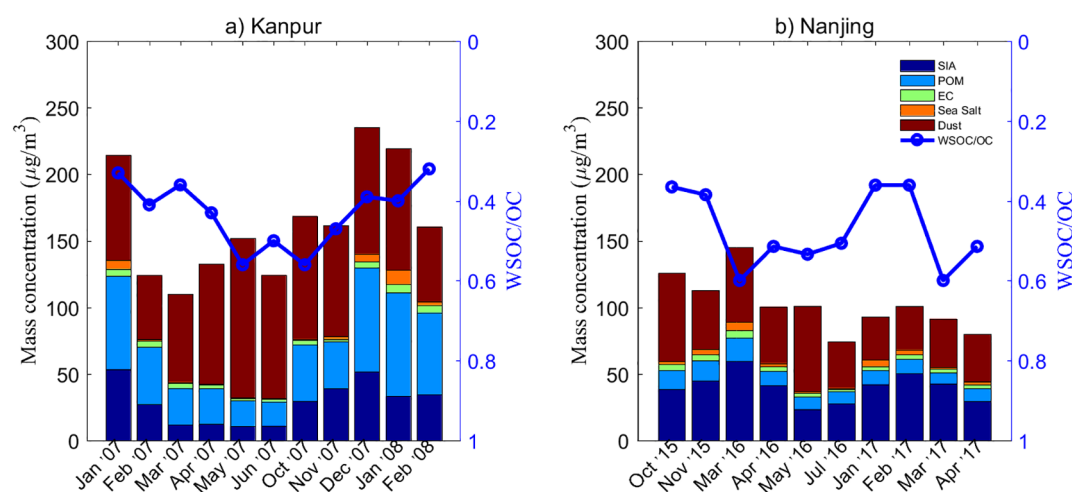


**Figure 1.** Monthly mean mass concentrations of the five aerosol species converted from ion measurements and water-soluble OC (WSOC)/organic carbon (OC) ratios (the blue dotted line) obtained from the measurements in the (a) Kanpur and (b) Nanjing sites during the respective sampling periods.

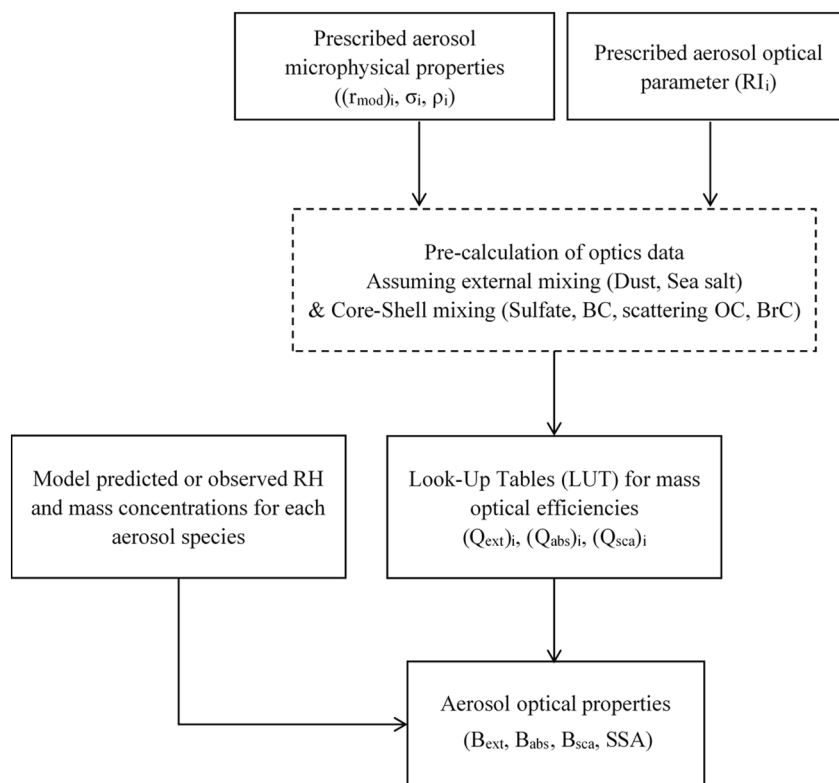


**Figure 2.** Schematic plot of the modified bulk aerosol optical scheme (BAOS). The subscript  $i$  indicates each of the six aerosol species among sulfate, black carbon (BC), scattering organic carbon (OC), brown carbon (BrC), sea salt, and dust. The dashed frame indicates the precalculation to generate the updated look-up table (LUT) of optics data for applying into BAOS.

### 3.2.3. Aerosol Mixing State

In the modified BAOS, four fine mode aerosols (sulfate, BC, scattering OC, and BrC) are assumed internally mixed (Core-Shell mixing), while dust and sea salt are still externally mixed as in the original BAOS. Therefore, the mass optical efficiencies of aerosol (e.g., the LUT of optics data) have to be recalculated. The updated LUT (see Text S1 and Table S3 in supplement) replaces the one in the original BAOS. The Core-Shell mixing refers to that BC absorbing core is coated with a mixture of sulfate, scattering OC, and BrC. The updated LUT was calculated with the formulation provided by Bohren and Huffman (1983) following the MIE theory (see Text S1 and Table S3 in supplement). Here we assumed the Core-Shell mixed particles had the same size distribution parameters as that of sulfate in the original BAOS ( $r_{\text{mod}} = 0.069 \mu\text{m}$ ,  $\sigma = 2.03$ ). A flowchart summarizes the aerosol optical calculation in the modified BAOS in Figure 2. The uncertainties associated with the mixing state and size distribution will be discussed in Sections 5.2.4, 5.2.5 and 6 respectively.

## 4. Methodology

### 4.1. Preparation for Closure Check

In order to evaluate the performance of modified BAOS, we run it standalone by utilizing aerosol measurement data in the two surface sites as inputs, then the outputs of modified BAOS are compared with observed aerosol optical data for a closure check. For inputs, the mass of each aerosol species is converted from the observed ionic concentrations and RH is obtained from automatic weather stations, to drive the modified BAOS. The outputs of surface aerosol optical properties are then compared with in situ observations. Normally, the relative bias between model outputs and observations within a considerable range (e.g., normally

below 30%) will be considered as achieving closure (Yuan et al., 2016), indicating an acceptable accuracy of model performance.

For the aerosol mass conversion, ammonium sulfate and ammonium nitrate aerosols are obtained from concentrations of  $\text{SO}_4^{2-}$  and  $\text{NO}_3^-$  (Tao et al., 2013). The sum of these two species is termed as secondary inorganic aerosol (SIA) and hereafter it will be referred to simply as sulfate aerosol as named in BAOS. Mass of particulate organic matter (POM) is calculated from the measured OC by multiplying it with a conversion factor (taken as 1.6 in this study, following R. Zhang et al., 2013). Note that POM mass applied in BAOS covers both the scattering POM (1.6 multiplies the mass of scattering OC) and BrC matter (obtained according to fBrC and the ratio of WSOC/OC in the modified BAOS as described in Section 3.2.2), EC aerosol from measurements is regarded as BC in BAOS. Sea salt mass concentrations are calculated from measured chloride ( $\text{Cl}^-$ ) (Pitchford et al., 2007). Mass of mineral dust is usually calculated from crustal elements, but they were not available in the onsite measurement. Therefore, we assume that the undefined mass (UM, refers to the difference between  $\text{PM}_{10}$  and the summed mass of the four identified aerosols) represents the dust aerosol (Ram & Sarin, 2011). It is pertinent to state here that UM can only be treated as an upper bound of dust mass concentrations. To sum up, the inputs of mass concentration for each aerosol species in the modified BAOS are calculated from the observed concentrations of chemical ions as the following equations:

$$\text{Sulfate} = \text{SIA} = 1.375 \times \text{SO}_4^{2-} + 1.29 \times \text{NO}_3^- \quad (1)$$

$$\text{Scattering POM} = 1.6 \times \text{OC} \times (1 - \text{fBrC} \times \text{WSOC/OC}) \quad (2)$$

$$\text{BrC matter} = 1.6 \times \text{OC} \times \text{fBrC} \times \text{WSOC/OC} \quad (3)$$

$$\text{BC} = \text{EC} \quad (4)$$

$$\text{Sea salt} = 1.82 \times \text{Cl}^- \quad (5)$$

$$\text{Dust} = \text{PM}_{10} - \text{Sulfate} - \text{POM} - \text{BC} - \text{SS} \quad (6)$$

Figure 1 plots the monthly mean mass concentrations of the five aerosol species (POM includes both scattering POM and BrC matter) at Kanpur and Nanjing after conversion. In the Kanpur site, dust fraction is high in spring and summer (March–June), which could be due to the long-range dust transport from Iran, Afghan, Pakistan, and the Thar Desert local in Western India (Ram et al., 2010a). POM dominates in fine mode, especially high in the fall and winter seasons due to biomass burning emissions. While in the Nanjing site, SIA (used as sulfate aerosol in BAOS) dominates in fine mode almost the whole time. EC and POM aerosols are relatively high in spring and autumn due to the burning of residual crops in this area (An et al., 2015; B. Li et al., 2015).

#### 4.2. Setup of Sensitivity Experiments

To investigate the impacts of BrC parameters on the uncertainties of total aerosol absorption in the modified BAOS, we perform sensitivity experiments by varying BrC parameters and as per the assumptions summarized in Table 2. The run with modified BAOS is referred to as a Control run. The sensitivity experiments can be divided into four groups according to the varying BrC property parameters: (a) including BrC absorption or not in Core-Shell mixing aerosol particles (Control run vs. Shell-nonBrC run); (b) varying  $K_{\text{BrC}}$  (Control run vs. Low-abs, High-abs run); (c) varying the prescribed mass ratio of BrC to WSOC (Control run vs. Sol-BrC run); (d) using different mixing assumptions for aerosol (Control run vs. Ext-mix run).

For the varying  $K_{\text{BrC}}$ , three sets of  $K_{\text{BrC}}$  (i.e., the imaginary RI in three bands covering near-ultraviolet, visible and near-infrared wavelength) are applied for sensitivity study. Low, medium, and high values of  $K_{\text{BrC}}$  are taken from collective observation and estimated values in currently available literature (summarized in Table 3). The variation of  $K_{\text{BrC}}$  for sensitivity experiments covers the widest range in BrC absorptivity (Table 2).

**Table 3**  
*A Summary of  $K_{BrC}$  Reported in Current Literature*

Band 11	Reference	Band 10	Reference	Band 9	Reference
0.009	Lack et al. (2012)	0.0019	Hoffer et al. (2006)	0.001	Kirchstetter et al. (2004)
0.015	Chakrabarty et al. (2010)	0.003	Chakrabarty et al. (2010)		
0.037	Shamjad et al. (2016)	0.016	Shamjad et al. (2016)		
0.112	Kirchstetter et al. (2004)	0.03	Kirchstetter et al. (2004)		
		0.06	Saleh et al. (2013)		

so that we can investigate its influence on aerosol absorption in the largest extension. The decreasing  $K_{BrC}$  from band 11 to band 9 indicates that BrC absorption is strongest in near-ultraviolet wavelengths and almost negligible in near-infrared. The difference in the simulated absorption between the Control run and Low-abs/High-abs run will provide a quantitative estimation of uncertainties due to BrC absorptivity in the modified BAOS.

For varying the BrC mass, Sol-BrC run increases the prescribed ratio of BrC to WSOC from 50% (Control run) to 100%, keeping all other BrC properties unchanged. Current literature indicates that BrC/WSOC is mostly between 0 and 1 in Asia (as summarized in Table 4), thus we take the median (50%) for the Control run and 100% for the sensitivity test (Sol-BrC run). The difference in the simulated absorption between the Control run and the Sol-BrC run will quantify the uncertainties root from the varying mass ratio of BrC to WSOC. Table 4 shows that BrC can be in water-insoluble OC (WIOC) too. We conduct an additional experiment (InSol-BrC run) and discuss the uncertainties associated with soluble/insoluble BrC in Section 5.2.3. Finally, a comparison between the Control run and the Ext-mix run shows the uncertainties attributed to the different mixing states of aerosol on absorption.

**Table 4**  
*A Summary of Mass Ratio of BrC to WSOC (and/or BrC to WIOC) Reported in Current Studies*

Methods	Ratio of BrC to WSOC or OC	Location	Time	Reference
CTM (IMPACT)	66% biofuel and biomass burning POA	Global	2000	Feng et al. (2013)
CTM (IMPACT)	100% POA from biofuel and biomass emissions and 100% SOA from biogenic and anthropogenic emissions	Global	For preindustrial and present day	Lin et al. (2014)
CTM (GEOS-Chem)	25% biomass burning and 50% biofuel POA and aromatic SOA	Global	2006–2011	X. Wang et al. (2014)
Measurement	0%–100% WSOC	Rondonia, Brazil	2002/09	Hoffer et al. (2006)
Measurement	0%–100% WSOC	Beijing, China	Summer and winter of 2009	Cheng et al. (2011)
Measurement	0%–100% WSOC	Beijing, China	2010/10–2011/11	Du et al. (2014)
Measurement	70%–90% WSOC	Korea	2015/06–2016/05	Jo et al. (2016)
Measurement	0%–100% WSOC	Kanpur, India	2015/12–2016/02	Satish et al. (2017)
Measurement	Part of WSOC and part of WIOC	Laboratory	N/A	Chen and Bond (2010)
Measurement	Part of WSOC and part of WIOC	Georgia, United States	Summer and fall of 2012	J. M. Liu et al. (2013)
Measurement	Part of WSOC and part of WIOC	Central USA	2012/05–2012/06	J. Liu et al. (2015)
Measurement	Part of WSOC and part of WIOC	Beijing, China	2013/01 and 2013/06	Yan et al. (2017)
Measurement	Part of WSOC and part of WIOC	Central Pacific and Atlantic Oceans	2017/01–2017/02, 2017/09–2017/10, and 2018/04–2018/05	Zeng et al. (2020)

Abbreviations: BrC, brown carbon; CTM, chemical transport model; OC, organic carbon; POA, primary organic aerosol; SOA, secondary organic aerosol; WIOC, water-insoluble OC; WSOC, water-soluble OC.

**Table 5**

Statistical Metrics to Compare the Simulated  $B_{abs}$  and AAE in Control Run With the Observations in the Kanpur and Nanjing Sites in Corresponding Wavelengths Ranges

Site	Wavelength (nm)	$B_{abs}$ ( $Mm^{-1}$ )				AAE			
		R	MRE (%)	RMB	RMSE	R	MRE (%)	RMB	RMSE
Kanpur	Control: 345–442	<b>0.833</b> (0.575, 0.288)	<b>34.89</b> (21.60, 58.15)	<b>1.129</b> (0.870, 1.582)	<b>36.03</b> (39.75, 28.38)	<b>-0.678</b> (-0.556, -0.916)	<b>15.33</b> (15.03, 15.84)	<b>0.957</b> (0.895, 1.065)	<b>0.198</b> (0.204, 0.187)
	OBS: 370								
	Control: 442–625	<b>0.794</b> (0.490, 0.129)	<b>31.36</b> (19.25, 52.54)	<b>1.123</b> (0.900, 1.513)	<b>21.50</b> (22.91, 18.80)				
	OBS: 520								
	Control: 625–778	<b>0.769</b> (0.456, 0.023)	<b>31.61</b> (19.96, 52.02)	<b>1.090</b> (0.884, 1.450)	<b>18.27</b> (19.85, 15.10)				
	OBS: 650								
	Control: 345–442	<b>0.765</b> (0.890, 0.850)	<b>16.16</b> (6.741, 22.43)	<b>1.100</b> (0.965, 1.191)	<b>11.17</b> (4.869, 13.86)	<b>0.051</b> (0.836, 0.050)	<b>15.13</b> (4.639, 22.13)	<b>1.136</b> (1.007, 1.221)	<b>0.220</b> (0.052, 0.280)
	OBS: 405								
Nanjing	Control: 625–778	<b>0.894</b> (0.980, 0.842)	<b>9.526</b> (5.991, 11.88)	<b>1.003</b> (0.940, 1.045)	<b>3.893</b> (2.762, 4.491)				
	OBS: 658								

Note. MRE and RMB in FW are mostly smaller than those in SS, because the observed values acting as the denominator are higher in FW and lower in SS (see Equations 8 and 9 in Section 4.3). Bolded numbers are metrics for the whole time period; the two numbers in the brackets are for FW and SS seasons, respectively.

Abbreviations: AAE, absorption Angstrom exponent; FW, fall and winter; MRE, mean relative error; R, correlation coefficient; RMB, relative mean bias; RMSE, root-mean-square error; SS, spring and summer.

### 4.3. Statistical Metrics

For evaluation purposes, simulation results of the modified BAOS (Control run) and all sensitivity experiments will compare with the observed aerosol absorption by utilizing statistical metrics. Monthly averaged  $B_{abs}$  in Kanpur are available at 370, 520, and 660 nm, and at 405 and 658 nm in Nanjing, due to the different instrumentations. We take the observed  $B_{abs}$  at 370 nm in Kanpur and that at 405 nm in Nanjing to compare with the simulated  $B_{abs}$  in band 11 (345–442 nm, see Table 5). Observed  $B_{abs}$  at 520 nm in Kanpur is compared with simulated  $B_{abs}$  in band 10 (442–625 nm, see Table 5). Observed  $B_{abs}$  at 660 nm in Kanpur and that at 658 nm in Nanjing are compared with the simulation result in band 9 (625–778 nm, see Table 5).

Aerosol spectral absorption is usually represented by AAE, which is calculated with  $B_{abs}$  at two different wavelengths ( $\lambda 1$  and  $\lambda 2$ ):

$$\text{AAE} = -\frac{\ln(B_{abs}(\lambda 1)/B_{abs}(\lambda 2))}{\ln(\lambda 1/\lambda 2)} \quad (7)$$

In this study, we obtain AAE using observed  $B_{abs}$  at 370, 520, and 660 nm in Kanpur, and using observed  $B_{abs}$  at 405 and 658 nm in Nanjing. The simulated AAE is calculated using  $B_{abs}$  in band 11 and band 9 for comparison.

To quantitatively evaluate the simulated aerosol absorption in BAOS, we refer to several statistical metrics including mean relative error (MRE), relative mean bias (RMB), and root-mean-square error (RMSE) shown in Equations 8–10, as well as the correlation coefficient (R):

$$\text{MRE} = \frac{1}{n} \sum_{\text{month}} \frac{|SIM - OBS|}{OBS} \times 100\% \quad (8)$$

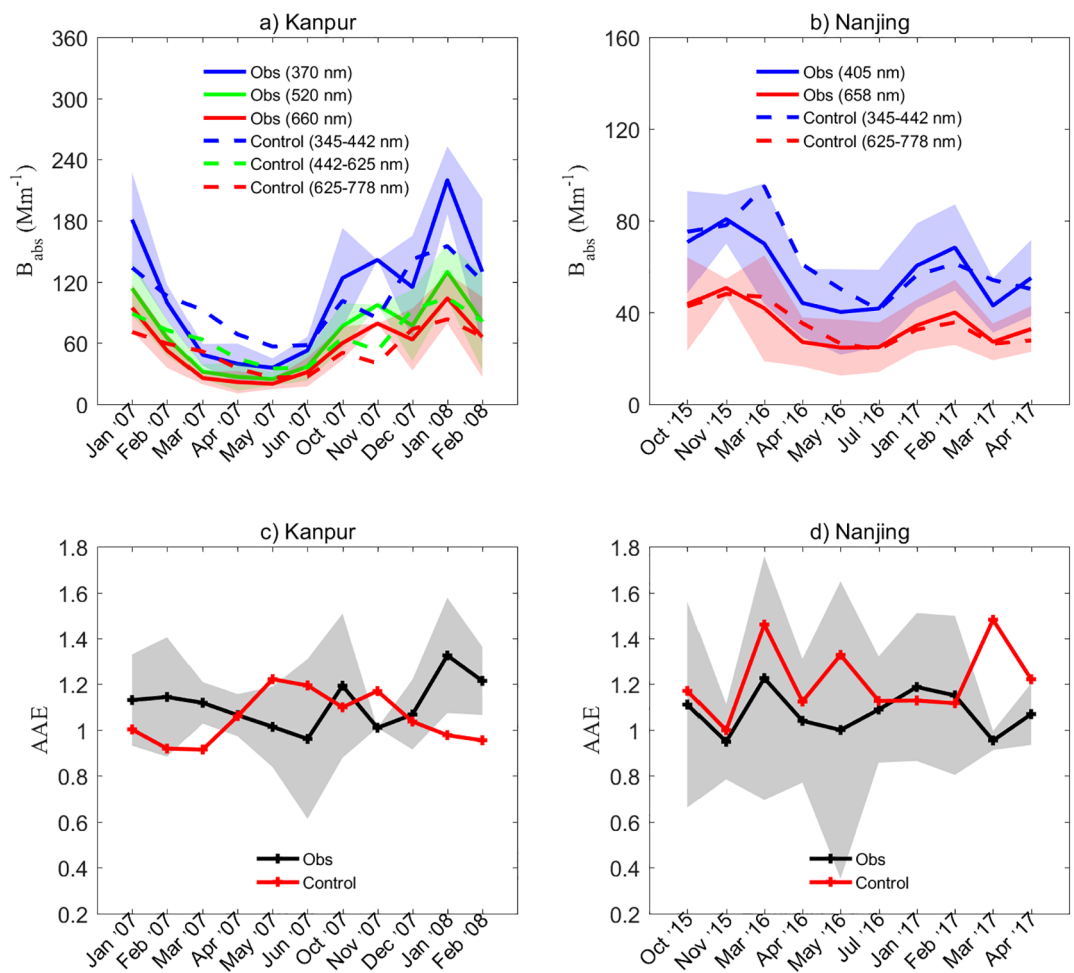


**Figure 3.** Comparison of simulated  $B_{\text{abs}}$  and absorption Angstrom exponent (AAE) in Control run with observed values in Kanpur and Nanjing. Shaded are one standard deviation for each monthly mean value of observations.

$$\text{RMB} = \frac{1}{n} \sum_{\text{month}} \frac{\text{SIM}}{\text{OBS}} \quad (9)$$

$$\text{RMSE} = \sqrt{\frac{1}{n} \sum_{\text{month}} (\text{SIM} - \text{OBS})^2} \quad (10)$$

where SIM and OBS refer to simulated and observed monthly mean quantities ( $B_{\text{abs}}$  or AAE) for aerosol absorption.  $n$  is the number of months with available observed data.

## 5. Results

### 5.1. Closure Check

Figure 3 shows the simulated  $B_{\text{abs}}$  and AAE from Control run, in comparison with the corresponding observed values. The observed  $B_{\text{abs}}$  in both sites show obvious seasonality, with peaks in the fall and winter seasons and troughs in the spring and summer seasons. High  $B_{\text{abs}}$  observed in fall and winter is consistent with the carbonaceous aerosol concentrations in Kanpur (Figure 1), which mainly originated from fossil-fuel and biomass burning activities and lower boundary layer height (Ram et al., 2010a). Based on this seasonal feature, we separate the results over fall and winter seasons (FW in short) and spring and summer seasons

(SS in short) for analysis. Statistical metrics for  $B_{\text{abs}}$  in different wavelengths and AAE over the different time periods for Kanpur and Nanjing are summarized in Table 5. On average, observed  $B_{\text{abs}}$  at 370 nm in Kanpur is underestimated by 5.76% and that in Nanjing is overestimated by 8.40% in the Control run. MRE is about 30%–35% in Kanpur and even below 20% in Nanjing during the whole periods, indicating a closure between model results and observation and acceptable accuracy of the modified BAOS in the urban pollution dominant site, but not in the biomass burning site (see Section 4.1).

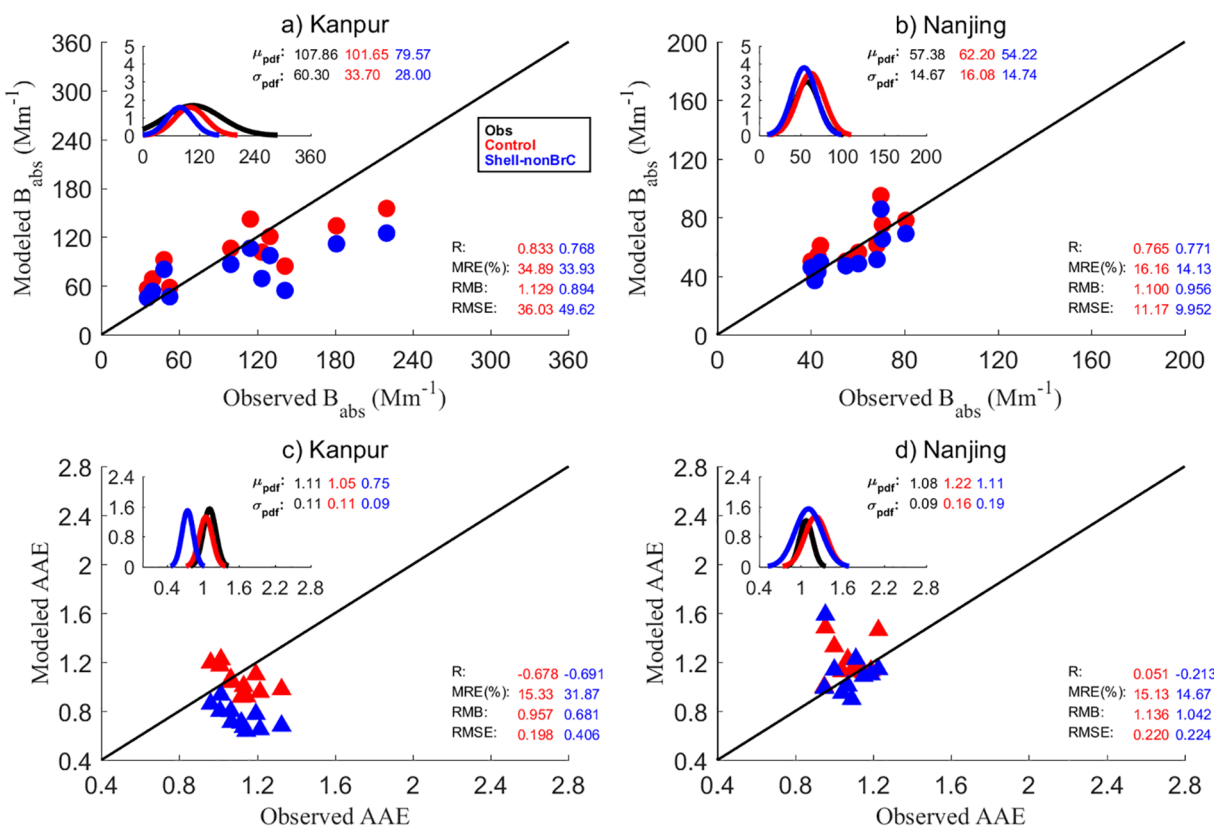
The modified BAOS roughly captures  $B_{\text{abs}}$  peaks in FW and troughs in SS in both sites, but significantly underestimates in FW and overestimates in SS seasons in Kanpur (Figure 3a). One possible explanation is that BrC absorptivity in FW seasons might be much stronger than we assumed in the Control run in a biomass-burning dominant region like Kanpur. Kirchstetter et al. (2004) ever derived the absorptivity of BrC extracted from biomass smoke samples collected in South Africa and indicated  $K_{\text{BrC}}$  is 0.112 at 400 nm, which is much higher than that of Control runs (0.037) over 345–442 nm. The discrepancy in  $B_{\text{abs}}$  caused by using a seasonally invariant  $K_{\text{BrC}}$  in the modified BAOS will be further discussed in Sections 5.2.2 and 5.3. The second reason for the underestimated  $B_{\text{abs}}$  in FW seasons could be the insufficient BrC mass amount calculated with the assigned BrC/WSOC fraction in the modified BAOS (see more discussions in Section 5.2.3). It should be noted that dust also contributes to the total aerosol absorption thus may partially compensate for the underestimated BrC absorption in model. We check the ratio of dust  $B_{\text{abs}}$  to total aerosol  $B_{\text{abs}}$ , which is 22% and 11% over SS and FW seasons in Kanpur respectively. Therefore, the overestimated  $B_{\text{abs}}$  in SS seasons could be attributed to high absorptivity or high ratio of BrC/WSOC assigned in model, or to dust absorption. To better quantify the discrepancy in BrC absorption in model, we would need more measurements of the physical and optical properties of dust aerosols to rule out the dust contribution to total aerosol absorption. But it is beyond the scope of this study.

Table 5 and Figures 3c and 3d show the comparison of simulated and observed AAE in Kanpur and Nanjing. The simulated AAE from the Control run and that from observations during the whole period are almost out of phase and have poor correlations at two sites. The discrepancies of AAE between simulations and observations may be caused by several factors. First, AAE was derived with  $B_{\text{abs}}$  at two or more different wavelengths. The underestimation of  $B_{\text{abs}}$  at the shorter wavelengths will cause an underestimation of AAE, such as in FW seasons in Kanpur. Second, the observed  $B_{\text{abs}}$  from Aethalometer could include dust absorption (although the dust absorption was assumed to be negligible in the measurements in Section 2.4). Therefore, we hardly rule out the uncertainties related to dust aerosol in the modified BAOS, as dust is referred to as the UM (Section 4.1) due to the lack of observational data. Dust could be another unnegelectable source for the discrepancies of  $B_{\text{abs}}$  and AAE, especially in SS seasons in Kanpur when dust absorption largely contributes to the total aerosol absorption (22%). Third, it should be noted that the AAE of carbonaceous aerosol can be less than one due to the particle size, shape, and mixing state. For example, Gyawali et al. (2009) showed that AAE smaller than one may result from BC coated with either absorbing or non-absorbing material. Lack and Cappa (2010) found that AAE less than one could happen, and the value of AAE depending on imaginary RI and diameters of core and shell of the mixed particle. Therefore the aerosol particle size parameters, mixing state and imaginary RI of carbonaceous aerosols that deviated from the real values during the measurement period will contribute to the discrepancy in AAE as well. On the other hand, the observed AAE in Nanjing is around 1 and shows a similar feature as urban aerosol in Bergstrom et al. (2007), who has discussed the AAE of different kinds of atmospheric aerosols and indicated that AAE was close to 1 for urban aerosol, but larger than 2 for biomass burning aerosol. The simulated AAE in Nanjing is overestimated in some spring months (March–May), which might be also related to the high dust contribution to the total aerosol  $B_{\text{abs}}$  (9%–20%) in this season.

## 5.2. Results of Sensitivity Experiments

### 5.2.1. BrC Inclusion

The influence of BrC absorption (or the brownness) in particle shells on total aerosol optical properties can be seen from the comparison between model (Control and Shell-nonBrC run) outputs and observational data (Figure 4). Average values and standard deviation of  $B_{\text{abs}}$  and AAE for observation and sensitivity experimental outputs at the two sites are summarized in Tables 6 and 7. In near-ultraviolet wavelength, total aerosol absorption is underestimated by about 26.23% in Kanpur and 5.51% in Nanjing when BrC



**Figure 4.** Comparison of  $B_{abs}$  in the near-ultraviolet wavelength and absorption Angstrom exponent (AAE) in Control and Shell-nonBrC runs with observed values. Subplot of each panel is the frequency distribution (#/bin) of  $B_{abs}$  or AAE. Statistical metrics (correlation coefficient [R], mean relative error [MRE], relative mean bias [RMB], and root-mean-square error [RMSE]) are calculated as described in Section 4.3.  $\mu_{pdf}$  and  $\sigma_{pdf}$  denote for the median value and standard deviation of the frequency distribution in the subplot.

absorption is not taken into account in particle shells (Shell-nonBrC run in Tables 6 and 7), decreasing by 20.47% and 13.91% in Kanpur and Nanjing compared with that of Control run. Averaged values of AAE from the Control run have better agreements with observations than Shell-nonBrC run at both sites. This

**Table 6**  
Multiple-Month Average of  $B_{abs}$  and AAE ( $\pm 1$  Standard Deviation) for the Observation and All Sensitivity Experiments at the Kanpur Site

	$B_{abs}$ (Mm $^{-1}$ )			AAE
Obs. wavelength (nm)	370 nm	520 nm	650 nm	
Observation	107.86 ( $\pm 60.30$ )	69.06 ( $\pm 35.96$ )	56.11 ( $\pm 29.17$ )	1.11 ( $\pm 0.11$ )
Model wavelength range (nm)	345–442 nm	442–625 nm	625–778 nm	
Control	101.65 ( $\pm 33.70$ )	66.89 ( $\pm 23.47$ )	52.95 ( $\pm 19.45$ )	1.05 ( $\pm 0.11$ )
Shell-nonBrC	79.57 ( $\pm 28.00$ )	59.13 ( $\pm 22.30$ )	50.43 ( $\pm 19.79$ )	0.75 ( $\pm 0.09$ )
Low-abs	86.75 ( $\pm 28.66$ )	62.00 ( $\pm 21.92$ )	52.95 ( $\pm 19.45$ )	0.81 ( $\pm 0.09$ )
High-abs	135.43 ( $\pm 46.43$ )	81.18 ( $\pm 28.30$ )	52.95 ( $\pm 19.45$ )	1.45 ( $\pm 0.13$ )
Sol-BrC	119.03 ( $\pm 40.02$ )	70.34 ( $\pm 25.20$ )	50.78 ( $\pm 19.65$ )	1.36 ( $\pm 0.19$ )
InSol-BrC	109.60 ( $\pm 45.04$ )	68.33 ( $\pm 27.30$ )	51.64 ( $\pm 20.18$ )	1.17 ( $\pm 0.10$ )
Ext-mix	107.88 ( $\pm 38.06$ )	72.97 ( $\pm 25.69$ )	53.98 ( $\pm 19.31$ )	1.07 ( $\pm 0.15$ )
PSD	83.72 ( $\pm 26.76$ )	56.71 ( $\pm 19.43$ )	45.08 ( $\pm 16.32$ )	1.00 ( $\pm 0.13$ )

Abbreviations: AAE, absorption Angstrom exponent; BrC, brown carbon; PSD, particle size distribution.

**Table 7**

Multiple-Month Average of  $B_{abs}$  and AAE ( $\pm 1$  Standard Deviation) for the Observation and All Sensitivity Experiments at the Nanjing Site

	$B_{abs}$ (Mm $^{-1}$ )	AAE
Obs. wavelength (nm)	370 nm	650 nm
Observation	57.38 ( $\pm 14.67$ )	34.67 ( $\pm 9.02$ )
Model wavelength range (nm)	345–442 nm	625–778 nm
Control	62.20 ( $\pm 16.08$ )	34.48 ( $\pm 8.80$ )
Shell-nonBrC	54.22 ( $\pm 14.74$ )	31.69 ( $\pm 8.82$ )
Low-abs	58.39 ( $\pm 15.01$ )	34.48 ( $\pm 8.80$ )
High-abs	71.46 ( $\pm 18.90$ )	34.48 ( $\pm 8.80$ )
Sol-BrC	65.40 ( $\pm 17.80$ )	32.09 ( $\pm 8.03$ )
InSol-BrC	62.37 ( $\pm 16.19$ )	34.01 ( $\pm 9.17$ )
Ext-mix	43.06 ( $\pm 11.99$ )	18.29 ( $\pm 5.58$ )
PSD	78.87 ( $\pm 20.69$ )	40.26 ( $\pm 10.39$ )

Abbreviations: AAE, absorption Angstrom exponent; BrC, brown carbon; PSD, particle size distribution.

estimated contribution of BrC brownness in particle shells to total aerosol absorption is comparable to that in previous studies. Feng et al. (2013) conducted three global calculations of aerosol optical properties with nonabsorbing OC (NON), moderately (MOD), and strongly (STR) absorbing BrC under the Core-Shell structure. On a global mean basis, the inclusion of the MOD BrC or STR BrC could enhance total aerosol absorption by 7% or 19% and led to more consistent AAE values with AERONET data. In our results, including BrC leads to noticeable improvements on simulated aerosol absorptive properties in Kanpur (Figure 4 shows that both  $B_{abs}$  and AAE frequency distributions are more similar to the observed ones), but has limited improvements in Nanjing site. However, BrC inclusion still underestimates the aerosol absorption in Nanjing (Table 5), mainly due to the failure of reproducing high absorption in fall and winter (Figure 3). BrC inclusion results in a slightly higher aerosol absorption in Nanjing (Figures 4b and 4d).

### 5.2.2. Imaginary RI of BrC

Contributions of the varying  $K_{BrC}$  to the simulated aerosol absorption are presented in Figure 5 and Tables 6 and 7 (Control vs. Low-abs, High-abs runs). In general, the larger the  $K_{BrC}$  is, the higher  $B_{abs}$  and AAE values are. Figure 5a and Figure S1a shows that High-abs run efficiently increases the aerosol absorption in FW seasons (when  $B_{abs}$  are larger than 100, see Figure 3a as well) and agrees better with the observed  $B_{abs}$  frequency distribution (subplot of Figure 5a). But Low-abs run matches better with the observed  $B_{abs}$  in SS seasons (when  $B_{abs}$  are smaller than 60, see Figure 3a and Figure S2a as well). The statistical metrics indicate that low absorbing BrC (Low-abs run) yields the smallest MRE by comparing with observational data over the whole measurement period (Figure 5a). In the Nanjing site, the three runs with different  $K_{BrC}$  have very similar  $B_{abs}$  and AAE outputs, which attribute to the relatively low amount of local carbonaceous aerosol emissions (see Figure 1).

As mentioned in the Introduction, two methods are currently used in simulating BrC in state-of-the-art global models. One is to isolate BrC from total organic matters and to calculate the absorption of BrC with assumed physical and optical properties (e.g.,  $K_{BrC}$ , the mass ratio of BrC to carbonaceous aerosol, and mixing state, as in this study). The other method is to parameterize the absorption of BrC as a function of the BC-to-OA ratio as described by Saleh et al. (2014). Lu et al. (2015) further verified this parameterization using multiple biomass burning samples in laboratory and field observations. This parameterization is favorable for being adopted in atmospheric models for biomass burning sources and providing a simultaneous and wide range of simulations, while it is unknown for other sources, for example, fossil fuel burning mostly occurred in cities. Our results in this subsection indicate that aerosol absorption is more sensitive to varying  $K_{BrC}$  in Kanpur, a location strongly influenced by biomass burning with strong seasonality, but is not susceptible to varying  $K_{BrC}$  in the urban site Nanjing, where city pollutions dominate. It again reminds

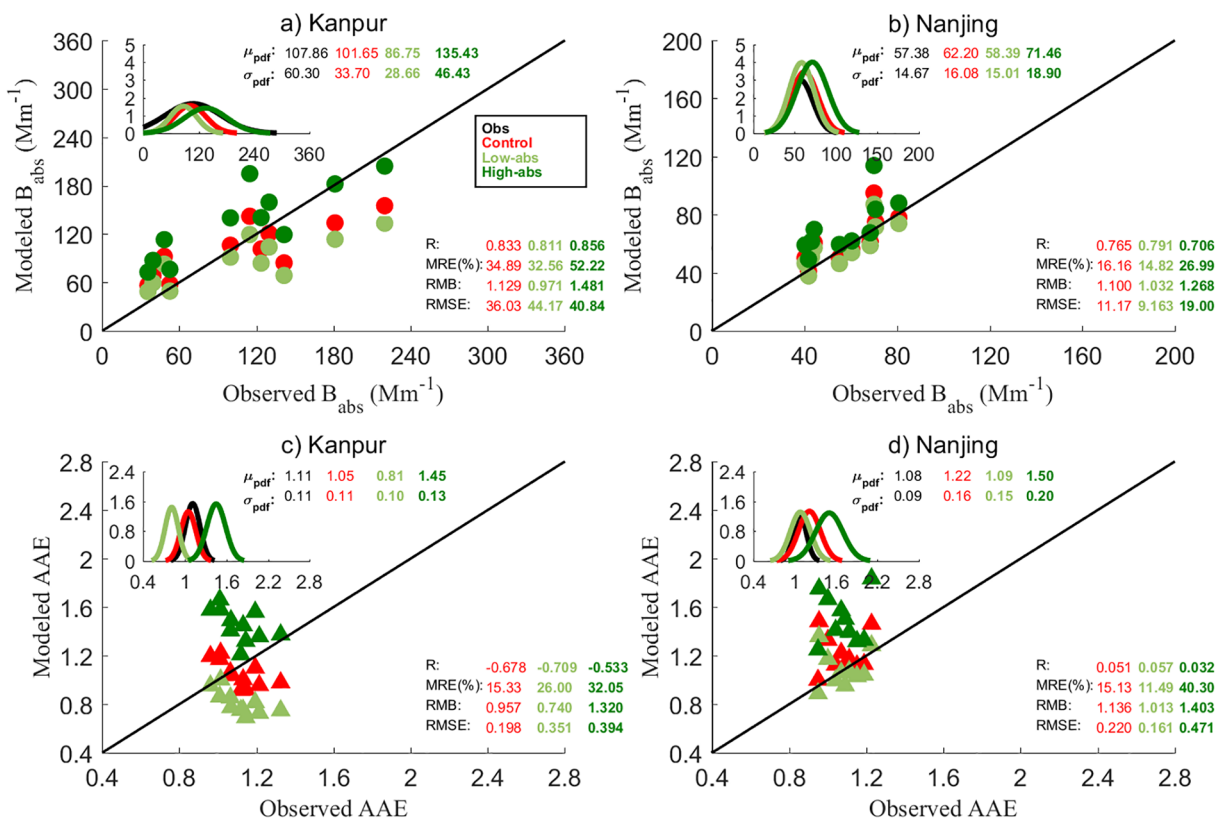


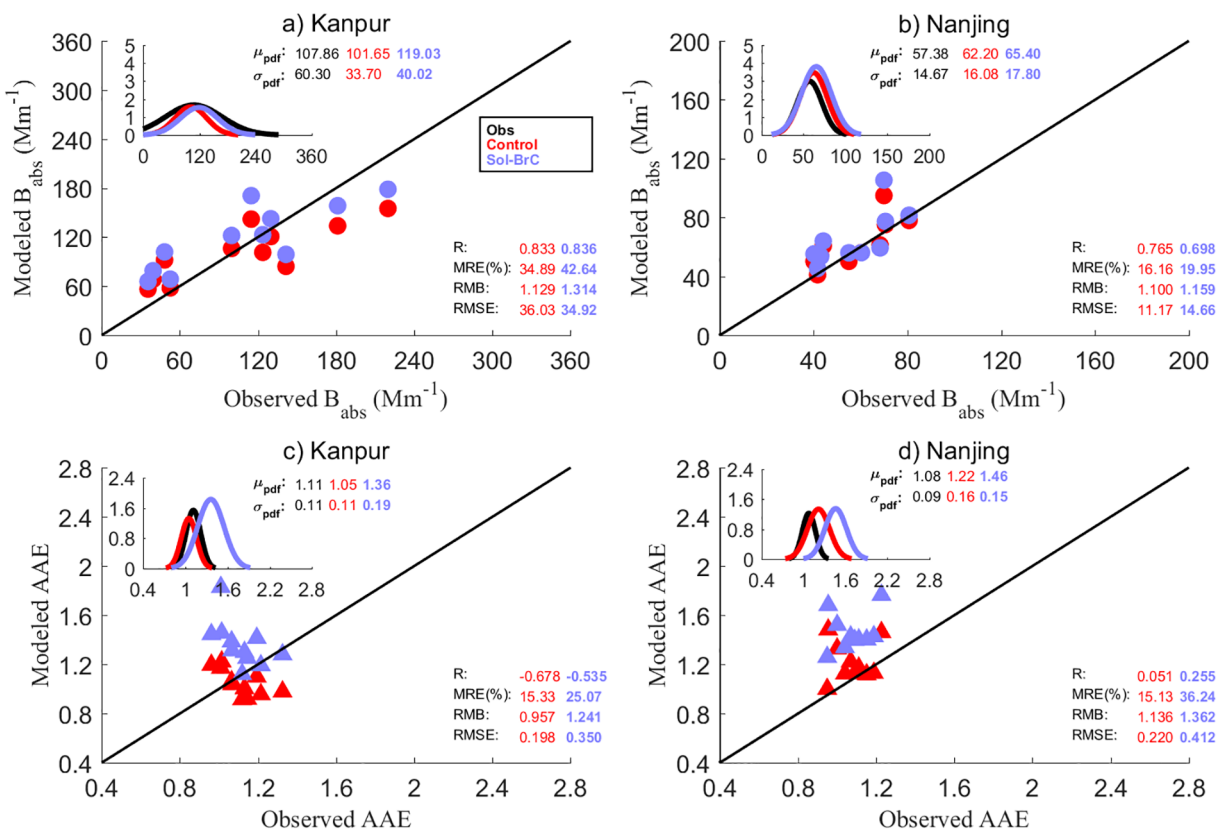
**Figure 5.** Comparison of  $B_{abs}$  in the near-ultraviolet wavelength and absorption Angstrom exponent (AAE) in Control, Low-abs, and High-abs runs with observed values. Subplot of each panel is the frequency distribution (#/bin) of  $B_{abs}$  or AAE. Statistical metrics (correlation coefficient [ $R$ ], mean relative error [MRE], relative mean bias [RMB], and root-mean-square error [RMSE]) are calculated as described in Section 4.3.  $\mu_{pdf}$  and  $\sigma_{pdf}$  denote for the median value and standard deviation of the frequency distribution in the subplot.

us that distinctive treatment of BrC optical calculation will be needed in the global model when considering the emission sources different from biomass burning.

### 5.2.3. Mass Ratio of BrC to WSOC

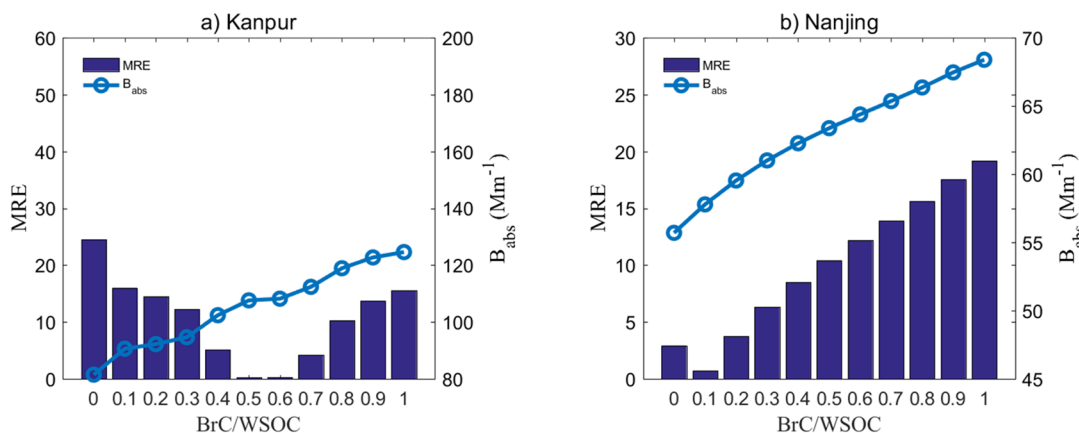
The impacts of the mass ratio of BrC to WSOC (BrC/WSOC) on the calculation of aerosol optical properties in the modified BAOS are presented in Figure 6 and Tables 6 and 7 (Control vs. Sol-BrC run). In the Kanpur site, a higher mass ratio of BrC in the model brings relatively stronger aerosol absorption, enhancing the correlation and the frequency distribution of simulated  $B_{abs}$  (Figure 6a). It is very likely related to the underestimated  $B_{abs}$  in FW seasons (see Figure 3a) and the increased BrC mass ratio enhances absorption thus counteracts the underestimation. In the Nanjing site, the varying ratio of BrC/WSOC makes little difference in simulated  $B_{abs}$  in near-ultraviolet wavelength due to the low amount of carbonaceous aerosol. However, Sol-BrC run efficiently shifts the AAE frequency distribution to a higher value. Overall speaking, Figure 6 indicates that assuming 100% WSOC as BrC in the model leads to insignificant changes in the simulated  $B_{abs}$ , but the noticeable shift toward higher AAE than assuming 50% WSOC as BrC.

Several observational studies have shown that BrC occupies a certain part of WSOC (Andreae & Gelencsér, 2006; Cheng et al., 2011; Du et al., 2014; Hoffer et al., 2006; Satish et al., 2017), but the measured mass ratio of BrC/WSOC in current literature is highly uncertain (Table 4). To further explore the dependence of aerosol absorption on the BrC/WSOC ratio, we repeat the Control run by varying BrC/WSOC from 0% to 100% with an interval of 10%. The simulated  $B_{abs}$  in the modified BAOS and MRE relative to the observation are plotted in Figure 7. In both sites,  $B_{abs}$  increases almost linearly with BrC/WSOC ratio, indicating the higher ratio of BrC results in stronger aerosol absorption. The best ratio for matching the overall observed  $B_{abs}$  is around 0.5, which is exactly the assumed ratio in the Control run in Kanpur, thus we can safely exclude the insufficient BrC mass amount as a reason for the underestimated  $B_{abs}$  in Figure 3a (Section 5.1).

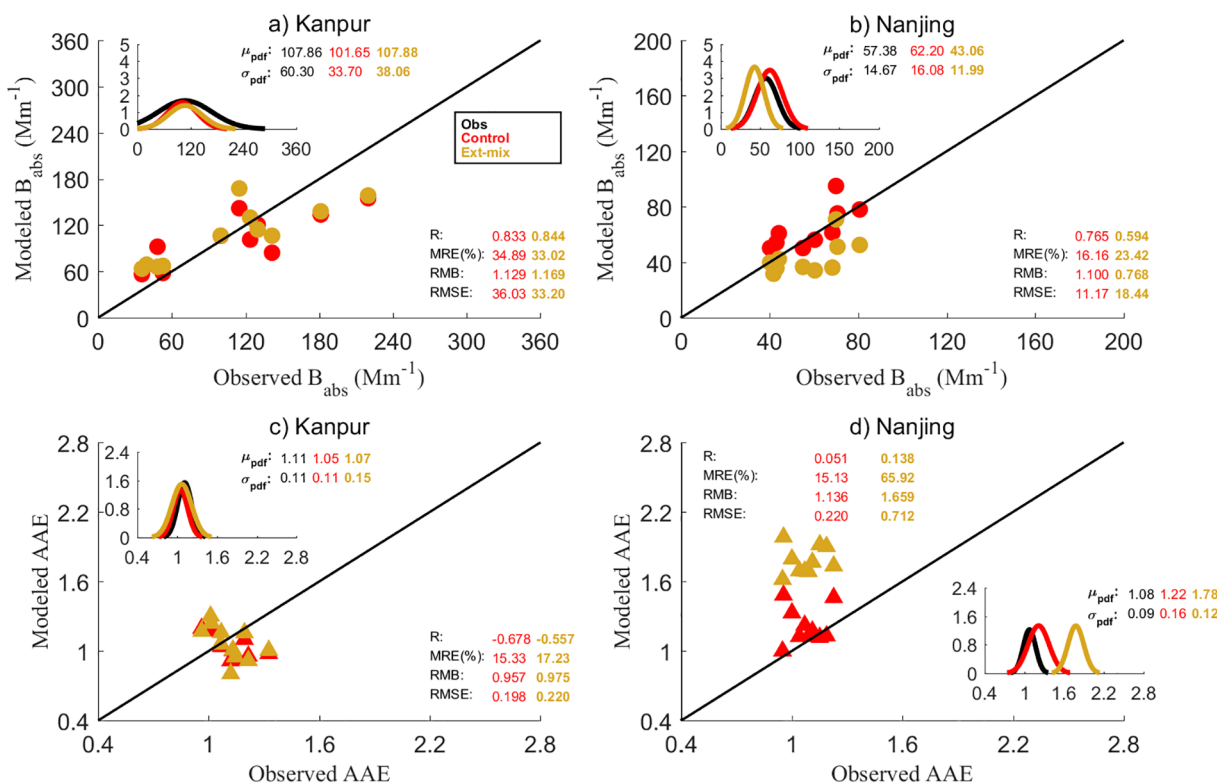


**Figure 6.** Comparison of  $B_{\text{abs}}$  in the near-ultraviolet wavelength and absorption Angstrom exponent (AAE) in Control and Sol-brown carbon (BrC) runs with observed values. Subplot of each panel is the frequency distribution (#/bin) of  $B_{\text{abs}}$  or AAE. Statistical metrics (correlation coefficient [ $R$ ], mean relative error [MRE], relative mean bias [RMB], and root-mean-square error [RMSE]) are calculated as described in Section 4.3.  $\mu_{\text{pdf}}$  and  $\sigma_{\text{pdf}}$  denote for the median value and standard deviation of the frequency distribution in the subplot.

As mentioned in Section 4.2 and Table 4, BrC can be found not only in WSOC but also in WIOC. Therefore we conduct an additional experiment by assuming BrC mass assigned as 50% WIOC mass (InSol-BrC). Simulated results and comparison with the Control run are shown in Figure S3. Generally speaking, differences in InSol-BrC and Control runs are trivial. It is because the assumption of soluble or insoluble BrC mainly influences the mass/volume ratio of BrC when calculating the optics of Core-Shell mixed particles (see



**Figure 7.**  $B_{\text{abs}}$  in the near-ultraviolet wavelength and mean relative error (MRE) (%) relative to observation with the varying mass ratio of brown carbon (BrC) in water-soluble OC (WSOC) in Control run at the two sites.



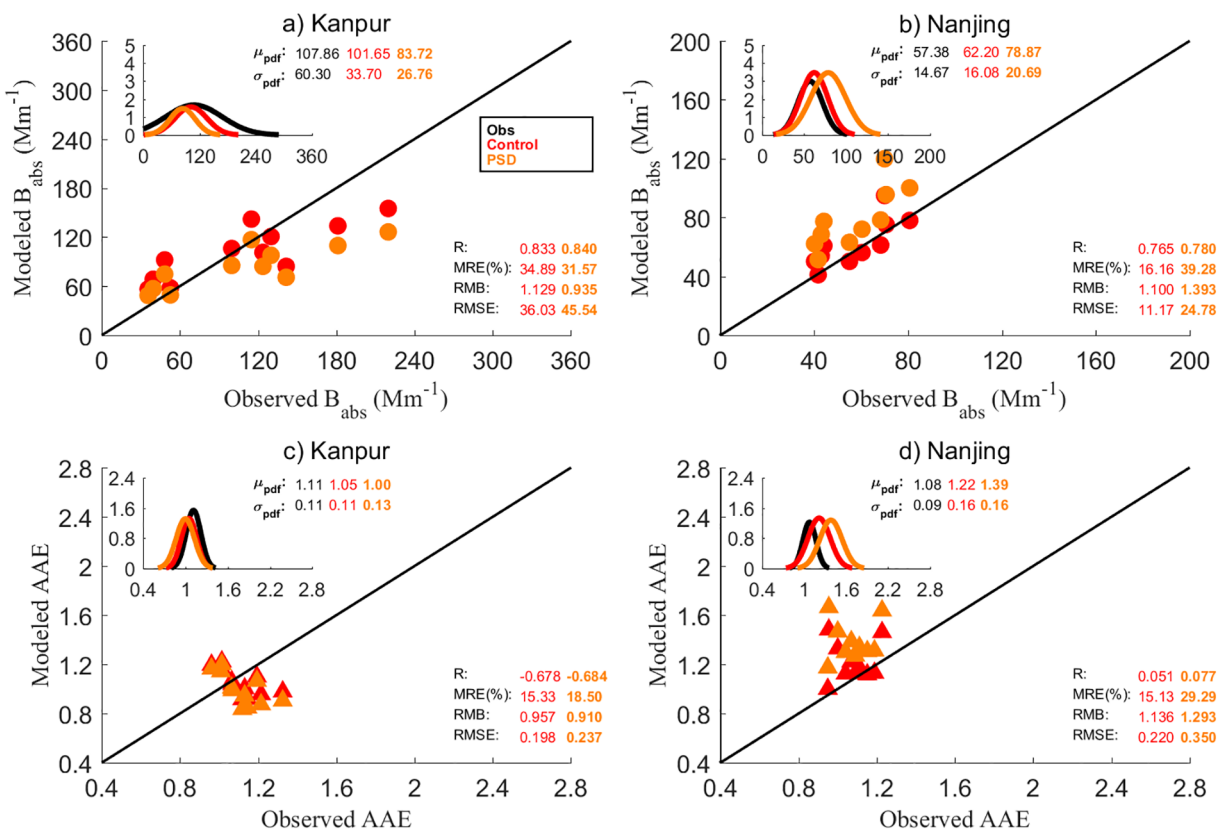
**Figure 8.** Comparison of  $B_{\text{abs}}$  in the near-ultraviolet wavelength and absorption Angstrom exponent (AAE) in Control and Ext-mix runs with observed values. Subplot of each panel is the frequency distribution (#/bin) of  $B_{\text{abs}}$  or AAE. Statistical metrics (correlation coefficient [ $R$ ], mean relative error [MRE], relative mean bias [RMB], and root-mean-square error [RMSE]) are calculated as described in Section 4.3.  $\mu_{\text{pdf}}$  and  $\sigma_{\text{pdf}}$  denote for the median value and standard deviation of the frequency distribution in the subplot.

Table S3 and caption in supplement), which has very limited effects on calculated aerosol optical properties while the aerosol size distribution is prescribed in BAOS.

The different mass ratios of BrC/WSOC or BrC/WIOC in the model not only impact the mass partition between BrC and scattering OC, but also the volume fractions of BrC and scattering OC in the Core-Shell mixture of aerosol due to the different density of BrC and scattering OC. These will further influence the calculated RI of the Core-Shell mixture and the hygroscopic growth of dry particles, and eventually on the optics of wet particles. The impacts of BrC/WSOC or BrC/WIOC ratio on the simulated aerosol absorption could be nonlinear and complex when the mass, size, and hygroscopicity of different aerosol species are varying with time and location. Although these parameters are simply prescribed in the modified BAOS for this study, more realistically assigned/simulated parameters in model will help to better represent these BrC properties. For example, A. Zhang et al. (2020) tried to estimate the temporal and spatial evolution of the BrC mass burden in a global model, avoiding using the prescribed uniform BrC mass ratio.

#### 5.2.4. Mixing State

Externally or internally mixed aerosol components have significant impacts on the simulated optical properties and hence the RF of atmospheric aerosols. Our results shown in Figure 8 and Tables 6 and 7 (Control vs. Ext-mix run) indicate that the Core-Shell mixture (Control run) yields stronger absorption than the external mixture, which means the reduction in lensing effect may be over-compensated by BrC shell absorption (Cheng et al., 2017; Luo et al., 2018). On the other hand, AAE in the Ext-mix run is overall stronger than that in the Control run (Figures 8c and 8d). Lack and Cappa (2010) investigated the influence of mildly absorbing coatings on the lensing effect. They showed that the reduction of the lensing effect was more evident in shorter wavelengths than in longer visible wavelengths. It is a possible explanation for the lower AAE in the Control run than in the Ext-mix run. Figure 8 shows that the internal mixing with Core-Shell structure yields more realistic outputs than the external mixing. This finding is similar to a previous study



**Figure 9.** Comparison of  $B_{\text{abs}}$  in the near-ultraviolet wavelength and absorption Angstrom exponent (AAE) in Control and particle size distribution (PSD) runs with observed values. Subplot of each panel is the frequency distribution (#/bin) of  $B_{\text{abs}}$  or AAE. Statistical metrics (correlation coefficient [ $R$ ], mean relative error [MRE], relative mean bias [RMB], and root-mean-square error [RMSE]) are calculated as described in Section 4.3.  $\mu_{\text{pdf}}$  and  $\sigma_{\text{pdf}}$  denote for the median value and standard deviation of the frequency distribution in the subplot.

by Tuccella et al. (2020). They conducted a 5-year global simulation with the GEOS-Chem model and calculated the aerosol optical properties for testing different mixing state assumptions of BC and BrC. Tuccella et al. (2020) found that the Core-Shell internal mixing representation produces the most accurate AAOD and SSA at the AERONET site dominated by carbonaceous absorption.

### 5.2.5. Particle Size Distribution

Aerosol size distribution could be a potential contributor to the uncertainties in the aerosol optical calculation, although it is prescribed in the modified BAOS under the framework of CAM5.3. To explore the sensitivity of calculated aerosol absorption on the variations of the particle size distribution (PSD), we conducted an additional experiment (PSD run) by replacing the fixed PSD with the PSD from measurements. The impacts of PSD on the calculation of aerosol optical properties in the modified BAOS are presented in Figure 9 and Tables 6 and 7 (Control vs. PSD run). Size distribution parameters ( $r_{\text{mod}}$ ,  $\sigma$ ) of fine particles in the two sites are obtained from AERONET (Dubovik & King, 2000) in Kanpur and from Sun-Sky Radiometer Observation Network (SONET, Z. Q. Li et al., 2018) in Nanjing. Both AERONET and SONET provided the retrieval product of volume median radius ( $r_v$ ), we converted it to number mode radius ( $r_{\text{mod}}$ ) following Equation 3 in J. Wang et al. (2012). Mean values of size distribution parameters ( $r_{\text{mod}}$ ,  $\sigma$ ) during observational periods in Kanpur and Nanjing are (0.091  $\mu\text{m}$ , 0.48) and (0.079  $\mu\text{m}$ , 0.58), respectively. The statistical metrics show that the uncertainties caused by varying PSD are substantial at both sites. Yet the simulated results in Control run by using the assumed PSD show better agreements with the observed distributions of  $B_{\text{abs}}$  and AAE.

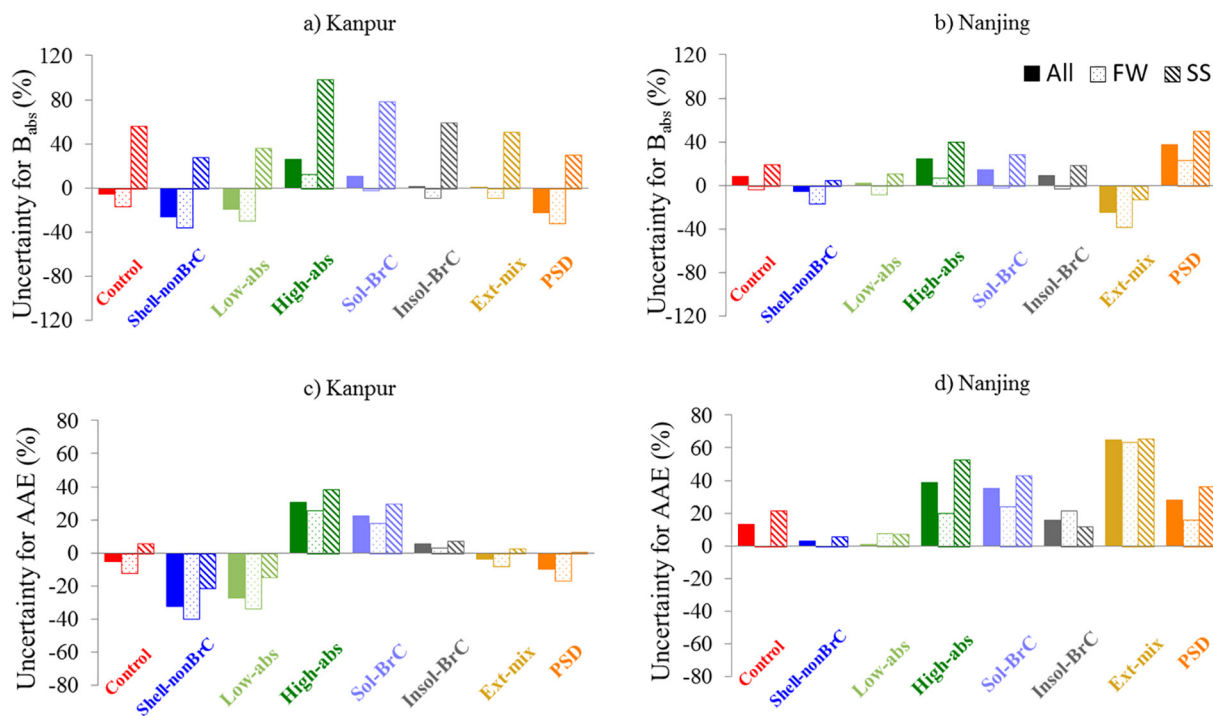


**Figure 10.** Uncertainties in  $B_{abs}$  and absorption Angstrom exponent (AAE) in Kanpur (a and c) and Nanjing (b and d) estimated by calculating the relative differences between the simulated results of each sensitivity experiment and the observed aerosol optical properties. Solid, dotted, and dashed bars are the uncertainties for the whole time period, fall and winter (FW) seasons and spring and summer (SS) seasons, respectively.

### 5.3. Analysis of Uncertainties

The uncertainties of  $B_{abs}$  and AAE resulted from various BrC parameters are plotted in Figure 10. The uncertainties are obtained by calculating the relative differences between the results of simulation experiments and the observed aerosol optical properties. The large uncertainties indicate that the corresponding varying BrC parameters have strong impacts on aerosol optical calculations. In the Kanpur site, whether including BrC or not has a noticeable impact on uncertainties in fall and winter seasons (Control and Shell-nonBrC runs in Figures 10a and 10c).  $K_{BrC}$  is the most significant influencing factor on uncertainties during the whole period. By applying high  $K_{BrC}$  in the fall and winter but low  $K_{BrC}$  in spring and summer helped to reduce the uncertainties of seasonal  $B_{abs}$  (Control, Low-abs, and High-abs runs in Figure 10a). Based on our analyses in the two Asian sites, we recommend focusing on more accurate representations (especially the seasonality) of BrC RI in biomass burning region (represented by Kanpur in this study). In the urban pollution dominated region (represented by Nanjing in this study), better understanding on aerosol mixing state and PSD (Figures 10b and 10d) would help to enhance the accuracy of simulation for aerosol optical properties in GCM.

## 6. Conclusions and Discussions

In this study, we aim to investigate the sources of BrC uncertainty in the aerosol optical calculation in a GCM. We first modified the BAOS in CAM5.3 by including BrC in the calculation for aerosol optical properties. The modified BAOS was run standalone being driven with observational aerosol data in two cities, Kanpur, India and Nanjing, China. A closure check was done for evaluating the performance of the modified BAOS. A series of sensitivity experiments were conducted to investigate the contribution of BrC inclusion, variations in imaginary RI ( $K_{BrC}$ ), BrC/WSOC ratio, mixing state of BrC, and aerosol PSD to the calculated aerosol absorption. The ranges of the varying BrC parameters were assigned according to former studies or current measurements. This study quantified the contributions of different BrC parameters to total aerosol absorption in the two Asian sites and attempted to identify the major BrC parameters responsible for uncertainties in total aerosol optical properties calculated in a climate model. By applying the observed

aerosol mass concentration as inputs to the modified BAOS, we ruled out the possible uncertainties introduced by emission or aerosol physical processes in model, and focused on the uncertainty sources related to BrC parameters in the aerosol optical calculation.

Our results showed that the simulation of Control run with the modified BAOS had an overall closure with observation in the Nanjing site (MRE within 20%) but an unsatisfactory closure in the Kanpur site (MRE around 35%). The simulated total aerosol absorption ( $B_{abs}$ ) in ultraviolet wavelengths generally captured the seasonal variability, except noticeable underestimations in fall and winter seasons and overestimations in spring and summer seasons in Kanpur. It indicates that a uniformly prescribed  $K_{BrC}$  in the modified BAOS might not be suitable for representing the seasonality of BrC absorption in the regions dominant with biomass burning. The simulated total aerosol absorption matched reasonably with observation (overall MRE within 20%) in Nanjing, where the urban pollution was dominant. The simulated AAE in Kanpur was underestimated in fall and winter and overestimated in spring and summer, which is possibly attributed to complex factors including the existence of dust aerosol and unneglectable dust absorption. In the Nanjing site, AAE was slightly overestimated in spring that is perhaps related to dust aerosol uncertainties, too. During the whole observation period, excluding BrC in the modified BAOS would reduce the simulated total aerosol absorption by about 20% and 14% in Kanpur and Nanjing, respectively. In addition, sensitivity experiments and relevant analyses indicated that variations in  $K_{BrC}$  had the strongest impacts on the uncertainties in calculated aerosol absorption in Kanpur, where biomass burning was dominant specifically in fall and winter. In contrast, the aerosol PSD and mixing state of BrC has the strongest impacts in Nanjing, where urban pollutions dominated for all seasons. In summary, we would like to draw modelers' attention to the strong seasonality of BrC absorptivity in biomass burning dominant region and the representations of size distribution and mixing state of fine particles (including BrC) in urban pollution dominant region. These were the major parameters significantly contributing to the uncertainties in the modeled total aerosol absorption in this study. We believed that more realistic (temporal or spatial varying) treatments on these BrC parameters would help to reduce the uncertainties in simulated RF of BrC in large-scale models.

Several points are noteworthy for discussion. First, we investigate the sensitivity of calculated aerosol absorption to the varying mass ratio of BrC to WSOC (Section 5.2.3) and briefly discuss its sensitivity to soluble/insoluble BrC. The uncertainties caused by varying BrC/WSOC from 50% to 100% are always stronger than that caused by varying from 50% BrC/WSOC to 50% BrC/WIOC (see Figure S3). The impacts of BrC mass ratio to soluble or insoluble OC on the uncertainties of aerosol absorption could be complex as it simultaneously interacted with mixing state and hygroscopic growth (as discussed in Section 5.2.3), thus more measurements to constrain these BrC properties would help for more realistic representations in model.

Second, we have considered only one internally mixing structure (Core-Shell) in the current study. Other mixing models could be applied to handle different types of internally mixed aerosols. For the case of insoluble particles suspended in solution, Maxwell-Garnett and Bruggeman mixing rules are two well-known methods (Lesins et al., 2002). The Maxwell-Garnett mixing rule assumes that a host material contains all other composite materials. While the Bruggeman mixing rule treats all materials on an equal base with the mixture of different components attached. H. Zhang et al. (2015) compared the impacts of three different internal mixing methods (Core-Shell, Maxwell-Garnett, and Bruggeman) with the external mixing method on aerosol optical properties and radiative flux. They found that the differences between the Core-Shell and Maxwell-Garnett/Bruggeman methods are usually larger than 15% in the near-ultraviolet and visible bands.

Third, laboratory and measurement studies show that BrC absorption can potentially decay under sunlight exposure with a lifetime of 1 h to 1 day, that is, chemical whitening or photo-bleaching effect (Forrister et al., 2015; H. J. Lee et al., 2014; X. Wang et al., 2016; Wong et al., 2019). Brown et al. (2018), X. Wang et al. (2018), and A. Zhang et al. (2020) considered the BrC photo-bleaching effect in their modeling work by applying a 1 day e-folding time or specifying a decay half-life in the aerosol chemistry part of model, and validating their results with observations. As this study focuses on BAOS for aerosol optical calculation only, modification on the aerosol physical part to including the BrC photo-bleaching effect is beyond the scope. An investigation into the uncertainties caused by the photo-bleaching effect of BrC can be extended for future study.

Last, this study utilized the long-term observational data with concurrent measurements of aerosol chemical components, mass concentration and aerosol optical properties, to rule out the possible uncertainties from the model emission and aerosol physical calculation and to evaluate the performance of an isolated aerosol optical scheme, the modified BAOS. However, such long-term and multiple-variable aerosol datasets are very rare. The lack of dust aerosol data in the two sites also makes it difficult in understanding the uncertainties of aerosol absorption. We realized that the two-site measurement data used in this study had limited representativeness for biomass burning or urban polluted regions. Moreover, we only simulated and analyzed surface aerosol optical properties in this study. Without aerosol data information in vertical coordinate, estimation on BrC RF and total aerosol RF are hardly constrained to real observations. In a word, we believed the more comprehensive datasets (ideally also including aircraft or satellite data with information of vertical distributions) in more extended BrC source regions over the global continents would help to better quantify the BrC uncertainties in the future study.

## Data Availability Statement

The source code of the bulk aerosol optical scheme for CAM5.3 can be accessed through a web browser [https://svn-ccsm-models.cgd.ucar.edu/cam1/release\\_tags/cesm1\\_2\\_1\\_n14\\_cam5\\_3\\_01/models/atm/cam/src/physics/cam/aer\\_rad\\_props.F90](https://svn-ccsm-models.cgd.ucar.edu/cam1/release_tags/cesm1_2_1_n14_cam5_3_01/models/atm/cam/src/physics/cam/aer_rad_props.F90). Particulate mass concentrations, OC/EC analysis, ionic species, optical measurements, and meteorological parameters in the Nanjing site can contact with Yanlin Zhang ([zhangyanlin@nuist.edu.cn](mailto:zhangyanlin@nuist.edu.cn)) and Mengying Bao ([baomy@nuist.edu.cn](mailto:baomy@nuist.edu.cn)). Those measurements in the Kanpur site are available in Ram et al. (2010a). Simulation results and observational data plotted and analyzed in this study are available at <https://zenodo.org/record/4762180#.YJ-T-1VKjIU>.

## Acknowledgments

This study is supported by the National Natural Science Foundation of China (grant number 41761144056, 41605106, and 41775137) and the National Important Project of the Ministry of Science and Technology (grant number 2017YFC1501404). Kirpa Ram thanks the Department of Science and Technology, Government of India for providing financial support under INSPIRE Faculty (#IFA-EAS-02) and SPICE-Climate Change Programme (DST/CCP/Aerosol/87/2017).

## References

- Alexander, D. T. L., Crozier, P. A., & Anderson, J. R. (2008). Brown carbon spheres in East Asian outflow and their optical properties. *Science*, 321(5890), 833–836. <https://doi.org/10.1126/science.1155296>
- An, J., Duan, Q., Wang, H., Miao, Q., Shao, P., Wang, J., & Zou, J. (2015). Fine particulate pollution in the Nanjing northern suburb during summer: Composition and sources. *Environmental Monitoring and Assessment*, 187(9), 561. <https://doi.org/10.1007/s10661-015-4765-2>
- Andreae, M. O., & Gelencser, A. (2006). Black carbon or brown carbon? The nature of light-absorbing carbonaceous aerosols. *Atmospheric Chemistry and Physics*, 6(10), 3131–3148. <https://doi.org/10.5194/acp-6-3131-2006>
- Arola, A., Schuster, G., Myhre, G., Kazadzis, S., Dey, S., & Tripathi, S. N. (2011). Inferring absorbing organic carbon content from AERONET data. *Atmospheric Chemistry and Physics*, 11(1), 215–225. <https://doi.org/10.5194/acp-11-215-2011>
- Bergstrom, R. W., Pilewskie, P., Russell, P. B., Redemann, J., Bond, T. C., Quinn, P. K., & Sierauf, B. (2007). Spectral absorption properties of atmospheric aerosols. *Atmospheric Chemistry and Physics*, 7(23), 5937–5943. <https://doi.org/10.5194/acp-7-5937-2007>
- Bikkina, S., Andersson, A., Ram, K., Sarin, M. M., Sheesley, R. J., Kirillova, E. N., et al. (2017). Carbon isotope-constrained seasonality of carbonaceous aerosol sources from an urban location (Kanpur) in the Indo-Gangetic Plain. *Journal of Geophysical Research: Atmospheres*, 122(9), 4903–4923. <https://doi.org/10.1002/2016JD025634>
- Bohren, C. F., & Huffman, D. R. (1983). *Absorption and scattering of light by small particles*. Wiley. <https://doi.org/10.1088/0031-9112/35/3/025>
- Bond, T. C. (2001). Spectral dependence of visible light absorption by carbonaceous particles emitted from coal combustion. *Geophysical Research Letters*, 28(21), 4075–4078. <https://doi.org/10.1029/2001gl013652>
- Bond, T. C., & Bergstrom, R. W. (2006). Light absorption by carbonaceous particles: An investigative review. *Aerosol Science and Technology*, 40(1), 27–67. <https://doi.org/10.1080/02786820500421521>
- Brown, H., Liu, X., Feng, Y., Jiang, Y., Wu, M., Lu, Z., et al. (2018). Radiative effect and climate impacts of brown carbon with the Community Atmosphere Model (CAM5). *Atmospheric Chemistry and Physics*, 18, 17745–17768. <https://doi.org/10.5194/acp-18-17745-2018>
- Chakrabarty, R. K., Moosmüller, H., Chen, L.-W. A., Lewis, K., Arnott, W. P., Mazzoleni, C., et al. (2010). Brown carbon in tar balls from smoldering biomass combustion. *Atmospheric Chemistry and Physics*, 10, 6363–6370. <https://doi.org/10.5194/acp-10-6363-2010>
- Chen, Y., & Bond, T. C. (2010). Light absorption by organic carbon from wood combustion. *Atmospheric Chemistry and Physics*, 10, 1773–1787. <https://doi.org/10.5194/acp-10-1773-2010>
- Cheng, Y., He, K., Engling, G., Weber, R., Liu, J., Du, Z., & Dong, S. (2017). Brown and black carbon in Beijing aerosols: Implications for the effects of brown coating on light absorption by black carbon. *Science of The Total Environment*, 599–600, 1047–1055. <http://dx.doi.org/10.1016/j.scitotenv.2017.05.061>
- Cheng, Y., He, K. B., Zheng, M., Duan, F. K., Du, Z. Y., Ma, Y. L., et al. (2011). Mass absorption efficiency of elemental carbon and water-soluble organic carbon in Beijing, China. *Atmospheric Chemistry and Physics*, 11(22), 11497–11510. <https://doi.org/10.5194/acp-11-11497-2011>
- Du, Z., He, K., Cheng, Y., Duan, F., Ma, Y., Liu, J., et al. (2014). A yearlong study of water-soluble organic carbon in Beijing II: Light absorption properties. *Atmospheric Environment*, 89, 235–241. <https://doi.org/10.1016/j.atmosenv.2014.02.022>
- Dubovik, O., & King, M. D. (2000). A flexible inversion algorithm for retrieval of aerosol optical properties from Sun and sky radiance measurements. *Journal of Geophysical Research*, 105(D16), 20673–20696. <https://doi.org/10.1029/2000JD900282>
- Feng, Y., Ramanathan, V., & Kotamarthi, V. R. (2013). Brown carbon: A significant atmospheric absorber of solar radiation? *Atmospheric Chemistry and Physics*, 13(17), 8607–8621. <https://doi.org/10.5194/acp-13-8607-2013>
- Forrister, H., Liu, J. M., Scheuer, E., Dibb, J., Ziembka, L., Thornhill, K. L., et al. (2015). Evolution of brown carbon in wildfire plumes. *Geophysical Research Letters*, 42, 4623–4630. <https://doi.org/10.1002/2015GL063897>

- Gyawali, M., Arnott, W. P., Lewis, K., & Moosmüller, H. (2009). In situ aerosol optics in Reno, NV, USA during and after the summer 2008 California wildfires and the influence of absorbing and non-absorbing organic coatings on spectral light absorption. *Atmospheric Chemistry and Physics*, 9(20), 8007–8015. <https://doi.org/10.5194/acp-9-8007-2009>
- Haywood, J. M., & Shine, K. P. (1995). The effect of anthropogenic sulfate and soot aerosol on the clear sky planetary radiation budget. *Geophysical Research Letters*, 22(5), 603–606. <https://doi.org/10.1029/95GL00075>
- Hecobian, A., Zhang, X., Zheng, M., Frank, N., Edgerton, E. S., & Weber, R. J. (2010). Water-soluble organic aerosol material and the light-absorption characteristics of aqueous extracts measured over the Southeastern United States. *Atmospheric Chemistry and Physics*, 10(13), 5965–5977. <https://doi.org/10.5194/acp-10-5965-2010>
- Hess, M., Koepke, P., & Schult, I. (1998). Optical properties of aerosols and clouds: The software package OPAC. *Bulletin of the American Meteorological Society*, 79(5), 831–844. [https://doi.org/10.1175/1520-0477\(1998\)079<0831:OPOAAC>2.0.CO;2](https://doi.org/10.1175/1520-0477(1998)079<0831:OPOAAC>2.0.CO;2)
- Hoffer, A., Gelencsér, A., Guyon, P., Kiss, G., Schmid, O., Frank, G. P., et al. (2006). Optical properties of humic-like substances (HULIS) in biomass-burning aerosols. *Atmospheric Chemistry and Physics*, 6(11), 3563–3570. <https://doi.org/10.5194/acp-6-3563-2006>
- Jacobson, M. Z. (2000). A physically-based treatment of elemental carbon optics: Implications for global direct forcing of aerosols. *Geophysical Research Letters*, 27(2), 217–220. <https://doi.org/10.1029/1999GL010968>
- Jacobson, M. Z. (2001). Strong radiative heating due to the mixing state of black carbon in atmospheric aerosols. *Nature*, 409(6821), 695–697. <https://doi.org/10.1038/35055518>
- Jo, D. S., Park, R. J., Lee, S., Kim, S. W., & Zhang, X. (2016). A global simulation of brown carbon: Implications for photochemistry and direct radiative effect. *Atmospheric Chemistry and Physics*, 16(5), 3413–3432. <https://doi.org/10.5194/acp-16-3413-2016>
- Kirchstetter, T. W., Novakov, T., & Hobbs, P. V. (2004). Evidence that the spectral dependence of light absorption by aerosols is affected by organic carbon. *Journal of Geophysical Research*, 109(21), 1–12. <https://doi.org/10.1029/2004JD004999>
- Kirchstetter, T. W., & Thatcher, T. L. (2012). Contribution of organic carbon to wood smoke particulate matter absorption of solar radiation. *Atmospheric Chemistry and Physics*, 12(14), 6067–6072. <https://doi.org/10.5194/acp-12-6067-2012>
- Kirillova, E. N., Sheesley, R. J., Andersson, A., & Gustafsson, Ö. (2010). Natural abundance <sup>13</sup>C and <sup>14</sup>C analysis of water-soluble organic carbon in atmospheric aerosols. *Analytical Chemistry*, 82(19), 7973–7978. <https://doi.org/10.1021/ac1014436>
- Lack, D. A., & Cappa, C. D. (2010). Impact of brown and clear carbon on light absorption enhancement, single scatter albedo and absorption wavelength dependence of black carbon. *Atmospheric Chemistry and Physics*, 10(9), 4207–4220. <https://doi.org/10.5194/acp-10-4207-2010>
- Lack, D. A., Langridge, J. M., Bahreini, R., Cappa, C. D., Middlebrook, A. M., & Schwarz, J. P. (2012). Brown carbon and internal mixing in biomass burning particles. *Proceedings of the National Academy of Sciences*, 109(37), 14802–14807. <https://doi.org/10.1073/pnas.1206575109>
- Laskin, A., Laskin, J., & Nizkorodov, S. A. (2015). Chemistry of atmospheric brown carbon. *Chemical Reviews*, 115(10), 4335–4382. <https://doi.org/10.1021/cr5006167>
- Lee, A. K. Y., Zhao, R., Li, R., Liggio, J., Li, S.-M., & Abbatt, J. P. D. (2013). Formation of light absorbing organo-nitrogen species from evaporation of droplets containing glyoxal and ammonium sulfate. *Environmental Science & Technology*, 47(22), 12819–12826. <https://doi.org/10.1021/es402687w>
- Lee, H. J., Aiona, P. K., Laskin, A., Laskin, J., & Nizkorodov, S. A. (2014). Effect of solar radiation on the optical properties and molecular composition of laboratory proxies of atmospheric brown carbon. *Environmental Science & Technology*, 48(17), 10217–10226. <https://doi.org/10.1021/es502515r>
- Lesins, G., Chylek, P., & Lohmann, U. (2002). A study of internal and external mixing scenarios and its effect on aerosol optical properties and direct radiative forcing. *Journal of Geophysical Research*, 107(D10). <https://doi.org/10.1029/2001jd000973>
- Li, B., Zhang, J., Zhao, Y., Yuan, S., Zhao, Q., Shen, G., & Wu, H. (2015). Seasonal variation of urban carbonaceous aerosols in a typical city Nanjing in Yangtze River Delta, China. *Atmospheric Environment*, 106, 223–231. <https://doi.org/10.1016/j.atmosenv.2015.01.064>
- Li, Z., Xu, H., Li, K., Li, D., Xie, Y., Li, L., et al. (2018). Comprehensive study of optical, physical, chemical, and radiative properties of total columnar atmospheric aerosols over China: An overview of Sun–Sky Radiometer Observation Network (SONET) measurements. *Bulletin of the American Meteorological Society*, 99(4), 739–755. <https://doi.org/10.1175/bams-d-17-0133.1>
- Lin, G., Penner, J. E., Flanner, M. G., Sillman, S., Xu, L., & Zhou, C. (2014). Radiative forcing of organic aerosol in the atmosphere and on snow: Effects of SOA and brown carbon. *Journal of Geophysical Research: Atmospheres*, 119(12), 7453–7476. <https://doi.org/10.1002/2013JD021186.Received>
- Liu, J., Bergin, M., Guo, H., King, L., Kotra, N., Edgerton, E., & Weber, R. J. (2013). Size-resolved measurements of brown carbon in water and methanol extracts and estimates of their contribution to ambient fine-particle light absorption. *Atmospheric Chemistry and Physics*, 13(24), 12389–12404. <https://doi.org/10.5194/acp-13-12389-2013>
- Liu, J., Scheuer, E., Dibb, J., Diskin, G. S., Ziembka, L. D., Thornhill, K. L., et al. (2015). Brown carbon aerosol in the North American continental troposphere: Sources, abundance, and radiative forcing. *Atmospheric Chemistry and Physics*, 15(14), 7841–7858. <https://doi.org/10.5194/acp-15-7841-2015>
- Liu, X., Zhang, Y. L., Peng, Y., Xu, L., Zhu, C., Cao, F., et al. (2019). Chemical and optical properties of carbonaceous aerosols in Nanjing, eastern China: Regionally transported biomass burning contribution. *Atmospheric Chemistry and Physics*, 19(17), 11213–11233. <https://doi.org/10.5194/acp-19-11213-2019>
- Lu, Z., Streets, D. G., Winjikul, E., Yan, F., Chen, Y., Bond, T. C., et al. (2015). Light absorption properties and radiative effects of primary organic aerosol emissions. *Environmental Science & Technology*, 49(8), 4868–4877. <https://doi.org/10.1021/acs.est.5b00211>
- Luo, J., Zhang, Y., Wang, F., & Zhang, Q. (2018). Effects of brown coatings on the absorption enhancement of black carbon: A numerical investigation. *Atmospheric Chemistry and Physics*, 18(23), 16897–16914. <https://doi.org/10.5194/acp-18-16897-2018>
- Mishra, S. K., & Tripathi, S. N. (2008). Modeling optical properties of mineral dust over the Indian Desert. *Journal of Geophysical Research*, 113(23), 1–19. <https://doi.org/10.1029/2008JD010048>
- Neale, R. B., Conley, A. J., Lauritzen, P. H., Williamson, D. L., Rasch, P. J., Vavrus, S. J., et al. (2010). *Description of the NCAR Community Atmosphere Model (CAM4.0)*. Boulder, CO: NCAR/TN-486+STR.
- Nie, W., Ding, A. J., Xie, Y. N., Xu, Z., Mao, H., Kerminen, V. M., et al. (2015). Influence of biomass burning plumes on HONO chemistry in eastern China. *Atmospheric Chemistry and Physics*, 15(3), 1147–1159. <https://doi.org/10.5194/acp-15-1147-2015>
- Park, R. J., Kim, M. J., Jeong, J. I., Youn, D., & Kim, S. (2010). A contribution of brown carbon aerosol to the aerosol light absorption and its radiative forcing in East Asia. *Atmospheric Environment*, 44(11), 1414–1421. <https://doi.org/10.1016/j.atmosenv.2010.01.042>
- Pitchford, M., Malm, W., Schichtel, B., Kumar, N., Lowenthal, D., & Hand, J. (2007). Revised algorithm for estimating light extinction from IMPROVE particle speciation data. *Journal of the Air & Waste Management Association*, 57(11), 1326–1336. <https://doi.org/10.3155/1047-3289.57.11.1326>

- Powelson, M. H., Espelien, B. M., Hawkins, L. N., Galloway, M. M., & De Haan, D. O. (2013). Brown carbon formation by aqueous-phase carbonyl compound reactions with amines and ammonium sulfate. *Environmental Science & Technology*, 48(2), 985–993, <https://doi.org/10.1021/es4038325>
- Ram, K., & Sarin, M. M. (2011). Day-night variability of EC, OC, WSOC and inorganic ions in urban environment of Indo-Gangetic Plain: Implications to secondary aerosol formation. *Atmospheric Environment*, 45(2), 460–468. <https://doi.org/10.1016/j.atmosenv.2010.09.055>
- Ram, K., & Sarin, M. M. (2015). Atmospheric carbonaceous aerosols from Indo-Gangetic Plain and Central Himalaya: Impact of anthropogenic sources. *Journal of Environmental Management*, 148, 153–163. <https://doi.org/10.1016/j.jenvman.2014.08.015>
- Ram, K., Sarin, M. M., & Hegde, P. (2008). Atmospheric abundances of primary and secondary carbonaceous species at two high-altitude sites in India: Sources and temporal variability. *Atmospheric Environment*, 42(28), 6785–6796. <https://doi.org/10.1016/j.atmosenv.2008.05.031>
- Ram, K., Sarin, M. M., & Tripathi, S. N. (2010a). A 1 year record of carbonaceous aerosols from an urban site in the Indo-Gangetic Plain: Characterization, sources, and temporal variability. *Journal of Geophysical Research*, 115, D24313. <https://doi.org/10.1029/2010JD014188>
- Ram, K., Sarin, M. M., & Tripathi, S. N. (2010b). Inter-comparison of thermal and optical methods for determination of atmospheric black carbon and attenuation coefficient from an urban location in northern India. *Atmospheric Research*, 97(3), 335–342. <https://doi.org/10.1016/j.atmosres.2010.04.006>
- Rizzo, L. V., Artaxo, P., Müller, T., Wiedensohler, A., Paixão, M., Cirino, G. G., et al. (2013). Long term measurements of aerosol optical properties at a primary forest site in Amazonia. *Atmospheric Chemistry and Physics*, 13(5), 2391–2413. <https://doi.org/10.5194/acp-13-2391-2013>
- Roden, C. A., Bond, T. C., Conway, S., & Pinel, A. B. O. (2006). Emission factors and real-time optical properties of particles emitted from traditional wood burning cookstoves. *Environmental Science & Technology*, 40(21), 6750–6757. <https://doi.org/10.1021/es052080i>
- Saleh, R., Hennigan, C. J., McMeeking, G. R., Chuang, W. K., Robinson, E. S., Coe, H., et al. (2013). Absorptivity of brown carbon in fresh and photo-chemically aged biomass-burning emissions. *Atmospheric Chemistry and Physics*, 13(15), 7683–7693. <https://doi.org/10.5194/acp-13-7683-2013>
- Saleh, R., Marks, M., Heo, J., Adams, P. J., Donahue, N. M., & Robinson, A. L. (2015). Contribution of brown carbon and lensing to the direct radiative effect of carbonaceous aerosols from biomass and biofuel burning emissions. *Journal of Geophysical Research: Atmospheres*, 120(19), 10285–10296. <http://dx.doi.org/10.1002/2015jd023697>
- Saleh, R., Robinson, E. S., Tkacik, D. S., Ahern, A. T., Liu, S., Aiken, A. C., et al. (2014). Brownness of organics in aerosols from biomass burning linked to their black carbon content. *Nature Geoscience*, 7, 647–650. <https://doi.org/10.1038/ngeo2220>
- Satish, R., Shamjad, P., Thamban, N., Tripathi, S., & Rastogi, N. (2017). Temporal characteristics of brown carbon over the Central Indo-Gangetic Plain. *Environmental Science & Technology*, 51(12), 6765–6772. <https://doi.org/10.1021/acs.est.7b00734>
- Schaap, M., Otjes, R. P., & Weijers, E. P. (2011). Illustrating the benefit of using hourly monitoring data on secondary inorganic aerosol and its precursors for model evaluation. *Atmospheric Chemistry and Physics*, 11(21), 11041–11053. <https://doi.org/10.5194/acp-11-11041-2011>
- Shamjad, P. M., Tripathi, S. N., Thamban, N. M., & Vreeland, H. (2016). Refractive index and absorption attribution of highly absorbing brown carbon aerosols from an urban Indian City-Kanpur. *Scientific Reports*, 6, 37735. <https://doi.org/10.1038/srep37735>
- Tao, J., Cheng, T., Zhang, R., Cao, J., Zhu, L., Wang, Q., et al. (2013). Chemical composition of PM<sub>2.5</sub> at an urban site of Chengdu in southwestern China. *Advances in Atmospheric Sciences*, 30(4), 1070–1084. <https://doi.org/10.1007/s00376-012-2168-7>
- Tuccella, P., Curci, G., Pitari, G., Lee, S., & Jo, D. S. (2020). Direct radiative effect of absorbing aerosols: Sensitivity to mixing state, brown carbon, and soil dust refractive index and shape. *Journal of Geophysical Research: Atmospheres*, 125, 1–25. <https://doi.org/10.1029/2019JD030967>
- Updyke, K. M., Nguyen, T. B., & Nizkorodov, S. A. (2012). Formation of brown carbon via reactions of ammonia with secondary organic aerosols from biogenic and anthropogenic precursors. *Atmospheric Environment*, 63, 22–31. <https://doi.org/10.1016/j.atmosenv.2012.09.012>
- Wang, J., Zhao, Q., Cui, S., & Zhu, C. (2012). Assessment of aerosol modes used in the MODIS Ocean aerosol retrieval. *Journal of the Atmospheric Sciences*, 69(12), 3595–3605. <https://doi.org/10.1175/JAS-D-12-051.1>
- Wang, X., Heald, C. L., Liu, J., Weber, R. J., Campuzano-Jost, P., Jimenez, J. L., et al. (2018). Exploring the observational constraints on the simulation of brown carbon. *Atmospheric Chemistry and Physics*, 18(2), 635–653. <https://doi.org/10.5194/acp-18-635-2018>
- Wang, X., Heald, C. L., Ridley, D. A., Schwarz, J. P., Spackman, J. R., Perring, A. E., et al. (2014). Exploiting simultaneous observational constraints on mass and absorption to estimate the global direct radiative forcing of black carbon and brown carbon. *Atmospheric Chemistry and Physics*, 14(20), 10989–11010. <https://doi.org/10.5194/acp-14-10989-2014>
- Wang, X., Heald, C. L., Sedlacek, A. J., de Sá, S. S., Martin, S. T., Alexander, M. L., et al. (2016). Deriving brown carbon from multiwavelength absorption measurements: Method and application to AERONET and Aethalometer observations. *Atmospheric Chemistry and Physics*, 16(19), 12733–12752. <https://doi.org/10.5194/acp-16-12733-2016>
- Weingartner, E., Saathoff, H., Schnaiter, M., Streit, N., Bitnar, B., & Baltensperger, U. (2003). Absorption of light by soot particles: Determination of the absorption coefficient by means of aethalometers. *Journal of Aerosol Science*, 34(10), 1445–1463. [https://doi.org/10.1016/S0021-8502\(03\)00359-8](https://doi.org/10.1016/S0021-8502(03)00359-8)
- Wong, J. P. S., Tsagkaraki, M., Tsiodra, I., Mihalopoulos, N., Violaki, K., Kanakidou, M., et al. (2019). Atmospheric evolution of molecular-weight-separated brown carbon from biomass burning. *Atmospheric Chemistry and Physics*, 19(11), 7319–7334. <https://doi.org/10.5194/acp-19-7319-2019>
- Yan, C., Zheng, M., Bosch, C., Andersson, A., Desyaterik, Y., Sullivan, A. P., et al. (2017). Important fossil source contribution to brown carbon in Beijing during winter. *Scientific Reports*, 7, 43182. <https://doi.org/10.1038/srep43182>
- Yuan, J., Huang, X., Cao, L., Cui, J., Zhu, Q., Huang, C., et al. (2016). Light absorption of brown carbon aerosol in the PRD region of China. *Atmospheric Chemistry and Physics*, 16(3), 1433–1443. <https://doi.org/10.5194/acp-16-1433-2016>
- Zender, C. S., Bian, H., & David, N. (2003). Mineral Dust Entrainment and Deposition (DEAD) model: Description and 1990s dust climatology. *Journal of Geophysical Research*, 108(D14), 4416. <https://doi.org/10.1029/2002JD002775>
- Zeng, L., Zhang, A., Wang, Y., Wagner, N. L., Katich, J. M., & Joshua, P. (2020). Global measurements of brown carbon and estimated direct radiative effects. *Geophysical Research Letters*, 47(13), 1–11. <https://doi.org/10.1029/2020GL088747>
- Zhang, A., Wang, Y., Zhang, Y., Weber, R. J., Song, Y., Ke, Z., & Zou, Y. (2020). Modeling the global radiative effect of brown carbon: A potentially larger heating source in the tropical free troposphere than black carbon. *Atmospheric Chemistry and Physics*, 20(4), 1901–1920. <https://doi.org/10.5194/acp-20-1901-2020>
- Zhang, H., Zhou, C., Wang, Z., Zhao, S., & Li, J. (2015). The influence of different black carbon and sulfate mixing methods on their optical and radiative properties. *Journal of Quantitative Spectroscopy and Radiative Transfer*, 161, 105–116. <https://doi.org/10.1016/j.jqsrt.2015.04.002>

- Zhang, R., Jing, J., Tao, J., Hsu, S.-C., Wang, G., Cao, J., et al. (2013). Chemical characterization and source apportionment of PM<sub>2.5</sub> in Beijing: Seasonal perspective. *Atmospheric Chemistry and Physics*, 13(14), 7053–7074. <https://doi.org/10.5194/acp-13-7053-2013>
- Zhang, Y., & Cao, F. (2015). Fine particulate matter (PM<sub>2.5</sub>) in China at a city level. *Scientific Reports*, 5, 14884. <https://doi.org/10.1038/srep14884>
- Zhang, Y., Forrister, H., Liu, J., Dibb, J., Anderson, B., Schwarz, J. P., et al. (2017). Top-of-atmosphere radiative forcing affected by brown carbon in the upper troposphere. *Nature Geoscience*, 10, 486–489. <https://doi.org/10.1038/NGEO2960>